CURRENT FLOW IN THIN SOLID FILMS:
THERMIONIC EMISSION AND TUNNELING

Thesis by

Stephen L. Kurtin

In Partial Fulfillment of the Requirements

For the Degree of

Doctor of Philosophy

(Submitted September 18, 1970)

ACKNOWLEDGEMENTS

I would like to thank Carver Mead whose insight and enthusiasm have served as stimuli for this research; my wife, Barbara, whose understanding of the way in which the world, and her husband in particular, works is beyond parallel; the Hughes Aircraft Company and the Hertz Foundation whose generous financial support of my graduate education is deeply appreciated.

ABSTRACT

Current flow in metal-GaSe-metal sandwiches is investigated. These structures are particularly well suited to the study of current flow mechanisms because sandwiches containing uniform, single crystal films of gallium selenide can be easily fabricated. The well-defined nature of these structures allows sufficient a priori knowledge of their properties to make quantitative calculation of the predictions of appropriate models of current flow meaningful.

As discussed in Part I, for gallium selenide films between 200 Å and 1000 Å thick, experimentally observed currents are in excellent agreement with a simple model of thermionic contact-limited current flow. This investigation presents the first unequivocal evidence for contact-limited thermionic currents in solids.

In Part II films less than 100 Å thick are studied. For this thickness range, direct, inter-electrode tunneling is shown to be the dominant mechanism of current flow and an accurate energy-momentum dispersion relation within the forbidden gap of GaSe is obtained. This work represents the first quantitative calculation of tunneling currents in a metal-insulator-metal structure with all parameters relevant to the experiment independently determined.

TABLE OF CONTENTS

PART I

THERMIONIC CONTACT-LIMITED CURRENTS

I.1 INTRODUCTION

In this part we review the basic physics of contact-limited current flow and apply a simple model to the analysis of data obtained on well-defined MIM structures incorporating single crystal gallium selenide as the thin insulating film. The bulk and interface properties of gallium selenide were determined by independent experiments; these properties were used in the calculation of theoretical currents. No adjustable parameters were required. Both the magnitudes and functional dependencies of observed currents are in excellent agreement with theoretical predictions. Experimental variables include voltage, temperature, and insulator thickness. We believe that the excellent quantitative agreement obtained between theory and experiment provides the first unequivocal evidence for thermionic contact-limited transport in solids.

Section I.2 presents a brief perspective on the study of contact-limited currents. Section I.3 reviews experimental data previously obtained on bulk gallium selenide. These data, in conjunction with the discussion of sample preparation of Section I.4, are sufficient to fully describe the experimental specimens and hence to permit theoretical calculations of carrier transport phenomena without the need for curve fitting or the use of adjustable parameters. Section I.5 discusses criteria for the observation of contact rather than bulk-limited currents and applies these criteria to our experimental specimens. Section I.6

discusses a simple theory of contact-limited thermionic currents and compares the results of numerical calculations with experimental data obtained on Al-GaSe-Au structures. Excellent agreement is noted. Section I.7 presents direct evidence for image-force (Schottky) barrier lowering. In addition, this section includes a discussion of the energy distributions of carriers contributing to contact-limited current flow. These distributions give insight into the physical mechanisms which yield contact-limited currents.

I.2 BACKGROUND

Contact limited emission was first studied for the metal-vacuum interface. In this case three mechanisms of current flow may be distinguished:

1. Thermionic emission[1] (Schottky emission) occurs in the low field, high temperature limit and is a flux of electrons on the high-energy tail of the Maxwell-Boltzmann distribution over the image-force-lowered work function barrier.

2. Field emission[2,3] (Fowler-Nordheim tunneling) occurs in the high-field, low-temperature limit and is the direct quantum mechanical tunneling of electrons from allowed states below the Fermi level in a metal into allowed states in the vacuum.

3. Thermal-field emission[4-7] (T-F emission) occurs when the dominant contribution to the observed currents arises from the tunneling of thermally excited electrons through the narrow upper region of the image-force-lowered work function barrier. This mechanism of current flow is intermediate between thermionic emission and field emission.

Murphy and Good[8] showed that each of these mechanisms is a limiting approximation observed under appropriate conditions of applied field and temperature. Therefore, it is not in general fruitful to classify contact-limited currents into these various mechanisms because a significant portion of an observed current-voltage characteristic may, in physical situations, arise from regions of crossover from one mechanism to the next. Moreover, analytic integration of the equation of current

flow is not usually possible and hence numerical computation is used. To gain insight into the physics of carrier transport, one may also numerically evaluate the relative contribution to the current of carriers with various energies. Such energy distributions are considerably more informative than a mere classification of transport phenomena into the three cases outlines above.

Of course, even in metal-vacuum-metal structures, currents are not always contact limited. When more electrons are present in the vacuum region than can be collected in a transit time, build up of free charge in the vacuum region leads to the familiar space-charge-limited conduction in which the virtual cathode is spatially displaced from the physical cathode.

As interest in solids developed, it was natural to attempt analysis of current flow in solid state MIM structures. However, solid state insulators are far more complex than a vacuum and many additional factors must be taken into consideration. Two types of considerations arise:

a) the fundamental parameters of the insulator (e.g. carrier effective mass and dispersion relationship, dielectric constants, mobility-field relationship, interface barrier energies, trap densities and locations, etc.) must be known if meaningful predictions are to be made;

b) experimental techniques for preparing reproducible structures suitable for detailed study must be evolved.

These two types of considerations are not independent since values of the parameters used in theoretical treatments are often inferred

from the results of measurements on experimental structures.

Samples are usually fabricated by oxidation of a deposited metal film or by similar techniques. These techniques yield amorphous insulating films whose properties are ill-defined at best and are often spatially non-uniform. Current flow observed in such structures exhibits a generally exponential dependence on applied voltage and is often temperature dependent.[9-11] Since the bulk and interface properties of such insulating films are not known in detail, a rigorous matching of observed currents with a given model of carrier transport has not been possible. The usual procedure is to study the dependence of current on one or more variable (e.g. applied voltage, temperature, insulator thickness, electrode material, etc.), surmise an appropriate carrier transport mechanism or model, and then choose the parameters of the model (in fact these parameters are physical properties of the insulating film) so that the "predictions" of the model fit the observed currents. Great caution should be exercised when following such a procedure since physically distinct phenomena can lead to qualitatively similar behavior.[11] Even the distinctions between bulk and contact-limited current flow are blurred.[12] A real understanding of the underlying physics and its relevance to a given experimental situation can only be obtained from a detailed analysis of a well-defined experimental structure.

I.3 PROPERTIES OF GaSe

GaSe, used as the insulating material in all experiments reported here, is a layer compound having the crystal structure[13] shown in Fig. I.1. This structure consists of tightly internally bound four-fold (Se-Ga-Ga-Se) layers, stacked one on top of another to form a macro crystal held together by Van der Waals forces. As a result of this bonding configuration, it is possible to fabricate by peeling techniques thin film structures in which the single crystal character of the resulting GaSe thin film is maintained. Therefore, the properties of the GaSe film which is thus incorporated within a metal-GaSe-metal structure are necessarily identical with those of bulk GaSe crystals. The ability to incorporate a single crystal thin film in MIM structures permits interface, bulk, and thin film measurements to be performed on one and the same well-defined material.

To characterize the bulk properties of GaSe, several experimental techniques have been employed. Dielectric constants have been determined by both low-frequency and infrared measurements.[14] Capacitance measurements on thin, fully depleted samples indicate the low-frequency dielectric constant $K_{dc} = 8.0 \pm 0.3$ for the electric field parallel to the c-axis ($\mathcal{E} \parallel c$). Analysis of infrared reflectivity for each polarization of the electric vector yields $K_{opt} = 7.1$, $K_{dc} = 7.6$ for $\mathcal{E} \parallel c$; and $K_{opt} = 8.4$, $K_{dc} = 10.2$ for $\mathcal{E}_{\perp} c$. Multiple interference channeled spectra imply $K_{opt} = 7.45$ and $K_{dc} = 9.89$ for $\mathcal{E}_{\perp} c$.

Experiments on metal-GaSe interfaces yield other important data.

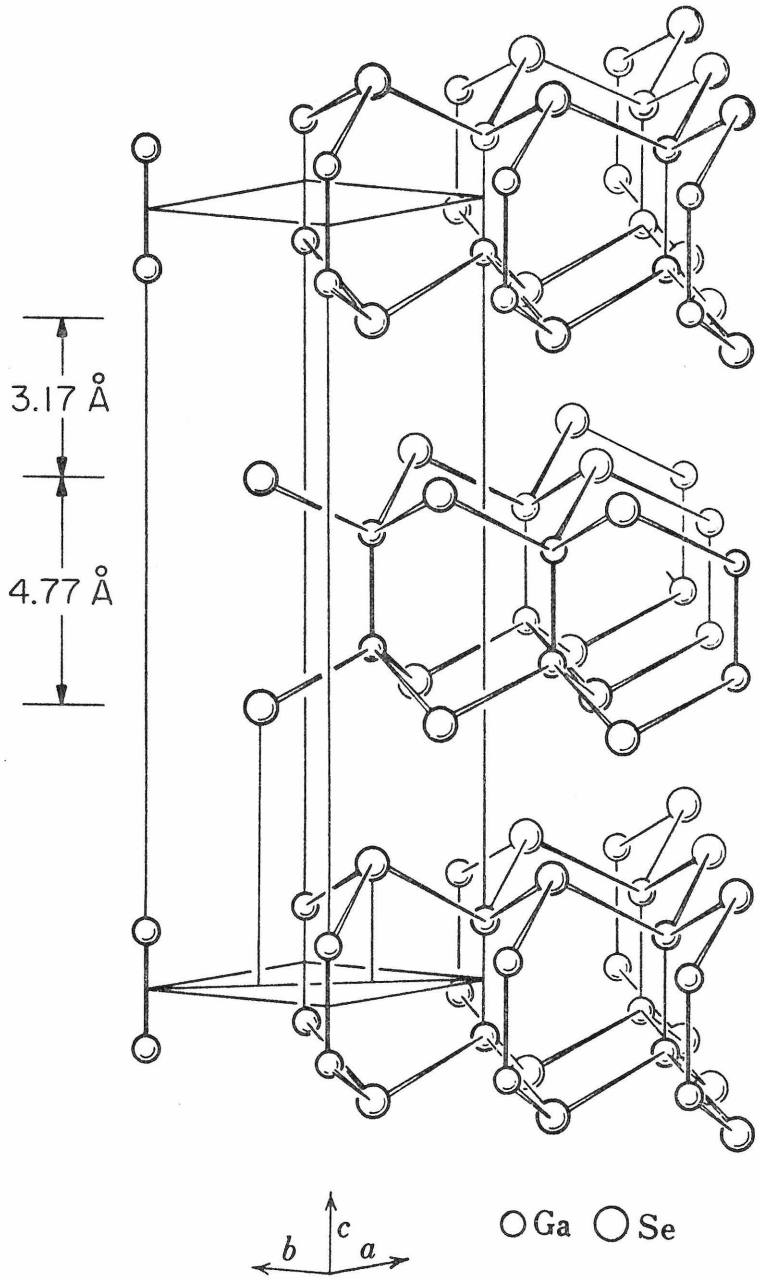

Fig. I.1 Schematic representation of the layer compound GaSe (after H. Kumimura and K. Nahao, Ref. 13). The tightly bound four-fold (Se-Ga-Ga-Se) layers are 4.77 Å across and are held together at an interlayer separation of 3.17 Å by predominantly Van der Waals forces. This material cleaves easily perpendicular to its c-axis thus facilitating the incorporation of a single crystal film within a MIM structure.

From measurements of capacitance as a function of voltage, our material was determined to be p-type with $p = 3 \times 10^{14}$ cm^{-3} at room temperature. Absorption edge measurements[15] indicate that the bandgap is 2.0 eV. In addition, photoresponse measurements at photon energies less than the band gap yield surface barrier energies[16] (i.e., the energy of the metal Fermi level above the GaSe valence band): Al-GaSe, $\phi_{Al} = 1.05$ eV; Au-GaSe, $\phi_{Au} = 0.52$ eV.

The relative importance of trapping states in bulk GaSe samples was appraised by determining (at constant applied bias) the sensitivity to broad-band optical radiation of the capacitance of metal-semiconductor interfaces (Schottky barrier depletion layer). No measurable change in capacitance was observed for the specimens used in this series of experiments, although material from highly doped ($p \simeq 10^{18}$ cm^{-3}) boules gave evidence of severe bulk trapping. In addition, measurements of capacitance as a function of frequency, performed on these same interfaces, failed to reveal any lifetime-dependent phenomena. This evidence for the absence of dominant bulk trapping indicates that $N_T << p$.

Tunneling measurements performed on metal-GaSe-metal structures incorporating a GaSe film less than 100 Å thick indicate that the tunneling effective mass for carriers near the valence band edge is approximately 0.1 of the free electron mass. Data obtained from tunneling experiments are qualitatively different[17] from those for the thicker films discussed here and comprise an independent study[18] which is the subject of Part II.

I.4 SAMPLE PREPARATION

Experimental structures used in this investigation were constructed by the following technique:

1) Approximately 1000 Å of metal (typically aluminum) was vacuum evaporated on one side of a freshly cleaved GaSe flake (≃ 5μ thick).

2) The flake was then mounted, metal side down, on a brass block. A 100% solids, silver loaded epoxy was used both to bond the flake to the block and to provide electrical contact to the evaporated metal layer.

3) The GaSe flake was peeled, in air,[19] to a thickness t (150 Å < t < 2000 Å; i.e., 20 to 250 integral Se-Ga-Ga-Se layers) by application of a flexible adhesive tape (Scotch Magic Transparent Tape) to the exposed upper GaSe surface. Care was taken to assure that a continuous GaSe film was removed with each successive peeling step, thereby eliminating the possibility of gross surface contamination by the tape adhesive.

4) Counterelectrodes of a metal (typically gold) were formed by vacuum evaporation through a fine mesh onto the freshly exposed (0001) surface. Each separate metallic dot defines an individual Al-GaSe-Au structure.

A schematic energy band representation of a typical (Al-GaSe-Au) structure is shown in Fig. I.2. By virtue of the incorporation of a single crystal thin film within the MIM sandwich, we are assured that the

physical parameters of the structure are well defined. Since the GaSe films in our specimens are much thinner than the zero bias, depletion layer thickness ($\simeq 1\mu$), the electric field within the structures is essentially uniform (in the absence of appreciable space charge, see Section I.6). Hence, Fig. I.2 is an accurate energy band representation.

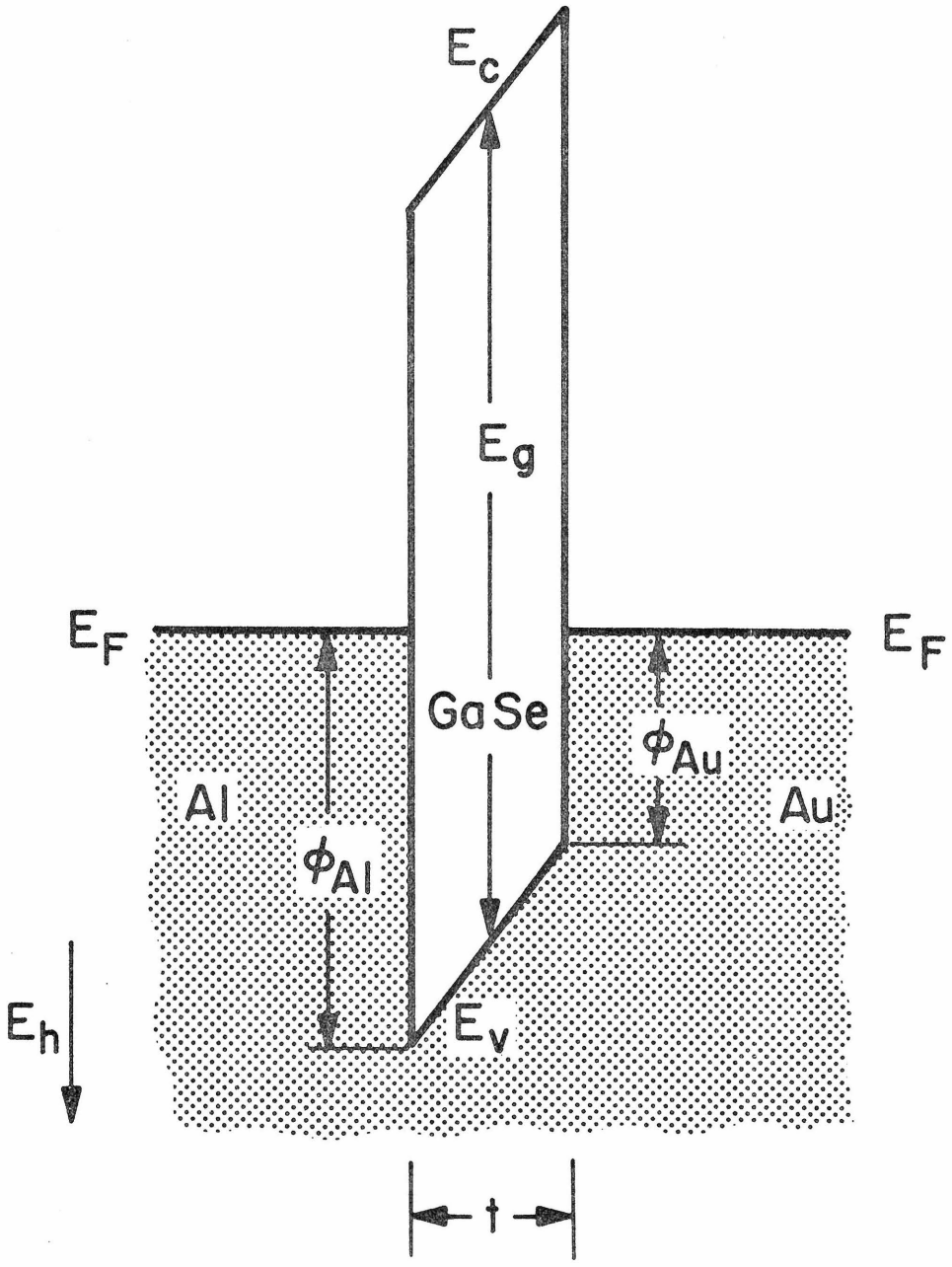

Fig. I.2 Energy band diagram of an Al-GaSe-Au structure under zero applied bias. Hole energy, E_h, increases down. E_g is the bandgap of GaSe, 2.0 eV. ϕ_{Al} is the Al-GaSe barrier energy, 1.05 eV; ϕ_{Au} is the Au-GaSe barrier energy, 0.52 eV. E_F denotes the Fermi level. As discussed in the text, this diagram is known to be accurate by virtue of the incorporation of a single crystal GaSe film within the structure.

I.5 BULK LIMITATIONS

In the absence of direct tunneling between the metal electrodes, current transport through MIM structures involves two serial processes. Carriers are injected into the insulator at the metal-insulator interface; they then traverse the insulating region. Either process can in principle limit the current. However, it is possible to define some criteria which, if fulfilled, insure that bulk limitations are not dominant. Bulk-limited currents can arise via two mechanisms: space charge and scattering (including for our purposes shallow trapping and other processes yielding low effective mobility).

Space charge limitations dominate carrier transport in MIM structures when the amount of uncompensated charge in the insulating region is sufficiently large to terminate a significant fraction of the field lines emanating from the metal electrodes. Both mobile charge (i.e., carriers in transit) and trapped charge contribute to this uncompensated charge. The mobile charge Q present in an insulator due to a current I is given by $Q = I\tau$, where τ is the time required for a charge carrier to transit the insulating film. If this charge is much less than the charge on the metal electrodes given by $Q_{electrode} = CV_T$, where C is the capacitance of the structure and V_T is the total voltage across the insulator (applied plus internal), then the space charge due to the mobile carriers is negligible. This condition is expressed by the inequality

$$I\tau < CV_T \qquad \text{(I.5-1)}$$

An upper bound on the contribution of trapped charge can be obtained from the total number of traps and the (worst case) assumption that all traps are ionized. Again, the criterion for neglecting the trapped space charge is that it be small compared to the total charge on the metal electrodes. The inequality

$$eN_t At < CV_T \qquad \text{(I.5-2)}$$

where e is the electronic charge, N_t is the density of traps, t is the thickness of the insulator, and A is the area of the structure, expresses this condition.

In those cases where the charge carriers traverse the insulator against the field before encountering the limiting barrier, both trapping and strong scattering may lead to deviations from the simple ballistic model of current transport discussed below.

If none of these mechanisms for bulk current limitation is present, the current will be contact-limited.

As noted in Section I.4, the GaSe film incorporated within a Au-GaSe-Al structure is single crystal material having the properties of bulk specimens. Thus, the criteria for observing contact-(as opposed to bulk) limited current can be checked in detail. For our material the number of traps is less than the acceptor density (as discussed in Section I.3) and hence the effect of the space charge due to ionized acceptors and deep traps can be estimated from the acceptor density. For $p \approx 3 \times 10^{14}$ cm^{-3} and $t \approx 500$ Å, the change in potential across the insulating layer due to ionized acceptors ($ept^2/2K_{opt}\varepsilon_o$) is less

than 10^{-3} eV. The influence of trapped charge on the barrier shape may thus be neglected.

The influence of space charge associated with current carriers in transit can be assessed on the basis of inequality I.5-1. By using data from experimental current-voltage characteristics and the structure capacitance, we may estimate an upper bound (τ_{ub}) on the value of the transit time for which space charge limitations are important, i.e., $\tau_{ub} = CV_T/I$. For a typical sample (the sample discussed in detail later in this section), τ_{ub} varies quite widely. However, (except for biases in the transition region from low forward to high forward where the field is nearly zero) the inequality is easily satisfied for physically reasonable values of effective carrier mobility. To illustrate this point, it is useful to express τ in terms of an effective mobility μ_{eff}: $\tau = t^2/\mu_{eff}\, V_t$ and to use the inequality $\tau < \tau_{ub}$ as a criterion for a lower bound (μ^o_{eff}) on the effective mobility. For μ_{eff} greater than this lower bound, charge associated with carriers in transit will not limit current flow. We find directly

$$\mu^o_{eff} = \frac{t^2 I}{CV_T^2} \qquad \text{(I.5-3)}$$

For samples discussed in this paper t^2/C is of order 1. Since μ^o_{eff} becomes large for large I and small V_T, we will choose a "worst" case close to flat band: $V_T = 0.1$ volt, $I = 10^{-6}$ amp. Therefore, $\mu^o_{eff} \simeq 10^{-4}$ cm^2/volt-sec; a value much below that expected for this material even perpendicular to the layers. Thus, currents observed in Au-GaSe-Al structures should be contact limited for all biases with the

possible exception of forward biases within 0.1 volts of $\phi_{Al} - \phi_{Au}$. Within 0.1 volts of $\phi_{Al} - \phi_{Au}$, the total internal field is small and hence space charge and other bulk limitations may be important.

I.6 CONTACT-LIMITED TRANSPORT

A. Barrier Shape

An important consideration in any discussion of contact-limited current is the assumed shape of the barrier potential. Simple discussions assume the barrier to be trapezoidal in shape, neglect the influence of space charge in the insulator, and correct the barrier shape for single or multiple image charges induced in the metal electrodes. In this approximation, including multiple image charges, the barrier potential is given by[4]

$$\phi(x) = \phi_1+(\phi_2-\phi_1-V)\frac{x}{t} - \frac{e}{16\pi K_{opt}\varepsilon_o x} - \frac{e}{8\pi K_{opt}\varepsilon_o t}\sum_{n=1}^{\infty}\frac{x^2}{n[(nt)^2-x^2]} \quad \text{(I.6-1)}$$

where I_{opt} is the optical dielectric constant of the insulator; t is the thickness of the insulating layer, ϕ_1 and ϕ_2 are the barrier energies, and V is the applied voltage.[20] Except for the small range of biases where the electric field in the barrier region is very nearly zero, charge transport is limited by the energy barrier at one of the metal-insulator interfaces (i.e., the limiting barrier). Consequently, approximations to the barrier potential which are accurate near the limiting barrier are appropriate to the discussion of contact-limited current. For definiteness, let us take the limiting barrier to be ϕ_1, and hence consider Eq. I.6-1 for x near zero. In the appendix we show that in this region the multiple image-force correction (the fourth term in Eq. I.6-1) may be neglected to very good approximation.[21] Thus, Eq. I.6-1 may be written

$$\phi(x) = \phi_o - \mathcal{E}x - \frac{e}{16\pi K_{opt}\, o\, x} \qquad (I.6\text{-}2)$$

where we have introduced ϕ_o for the limiting surface barrier energy and $\mathcal{E}$ for the total field acting near the limiting barrier.

B. Contact-Limited Current-Voltage Characteristics

In general, the total injection-limited current is the algebraic sum of four contributions: both holes and electrons may flow from either metal to the other. The relative importance of each of these contributions can be easily assessed using a simple thermionic model of carrier transport. To be specific, let us refer to the energy band diagram of Fig. I.2 wherein the electrode materials are gold and aluminum. Consider the case in which a negative bias V is applied to the gold electrode. (Other bias conditions may be discussed in an analogous manner). The hole current from Au-to-Al is proportional to $\exp[-(\phi_{Al}+V)/kT]$ while the hole current from Al-to-Au is proportional to $\exp(-\phi_{Al}/kT)$. Therefore, the ratio of the Au-to-Al hole current to the Al-to-Au hole current is equal to $\exp(-V/kT)$. Thus, for V greater than a few kT we can neglect the current contribution due to hole transport from Au-to-Al. Similarly, we find that for V greater than a few kT we can neglect the current contribution due to electron transport from Al-to-Au.

To assess the relative importance of hole current and electron current, we may use the same simple model. The dominant electron current is proportional to $\exp[-(E_g-\phi_{Au})/kT]$, where E_g is the band gap of the insulator; the dominant hole current is proportional to $\exp(-\phi_{Al}/kT)$.

Therefore, the ratio of hole current to electron current is given by $\exp[-(\phi_{Au}+\phi_{Al}-E_g)/kT]$. Thus, for $|\phi_{Au}+\phi_{Al}-E_g|>kT$ either hole or electron current must dominate. If $(\phi_{Au}+\phi_{Al}-E_g)>0$, electron current dominates; if $(\phi_{Au}+\phi_{Al}-E_g)<0$, hole current dominates.

In summary, if both the applied bias and the quantity $|\phi_{Au}+\phi_{Al}-E_g|$ are greater than a few kT then the major contribution to the total injection limited current comes from one and only one of the four possible contributions. Throughout the remainder of this paper, the above criteria will be satisfied for applied biases greater than 0.05 volt, since $|\phi_{Au}+\phi_{Al}-E_g| \sim 0.4$ eV $>>$ kT (kT $\simeq$ 0.025 eV at room temperature).

The current-voltage characteristic of an asymmetric ($\phi_{Au}<\phi_{Al}$) MIM structure in which current flow is contact-limited depends on two factors: the source of the current carriers, and the barrier which limits current flow. These two factors lead to a natural division of the current-voltage characteristic into three distinct regions depending upon which energy barrier is limiting current flow and which metal is supplying most of the current carriers. As illustrated by the solid curves and insets of Fig. I.3, these three distinct cases are "low forward," "high forward," and "reverse." Using the definition that positive bias results in current flow from gold to aluminum, we define the various cases in the following manner. Low forward occurs when positive bias is less than $\phi_{Al}-\phi_{Au}$. In this case the limiting barrier is the ϕ_{Al} barrier, the source of the current carriers is the gold electrode and current flows against the internal field. For the low forward, the current-voltage characteristic shows an exponential dependence of current

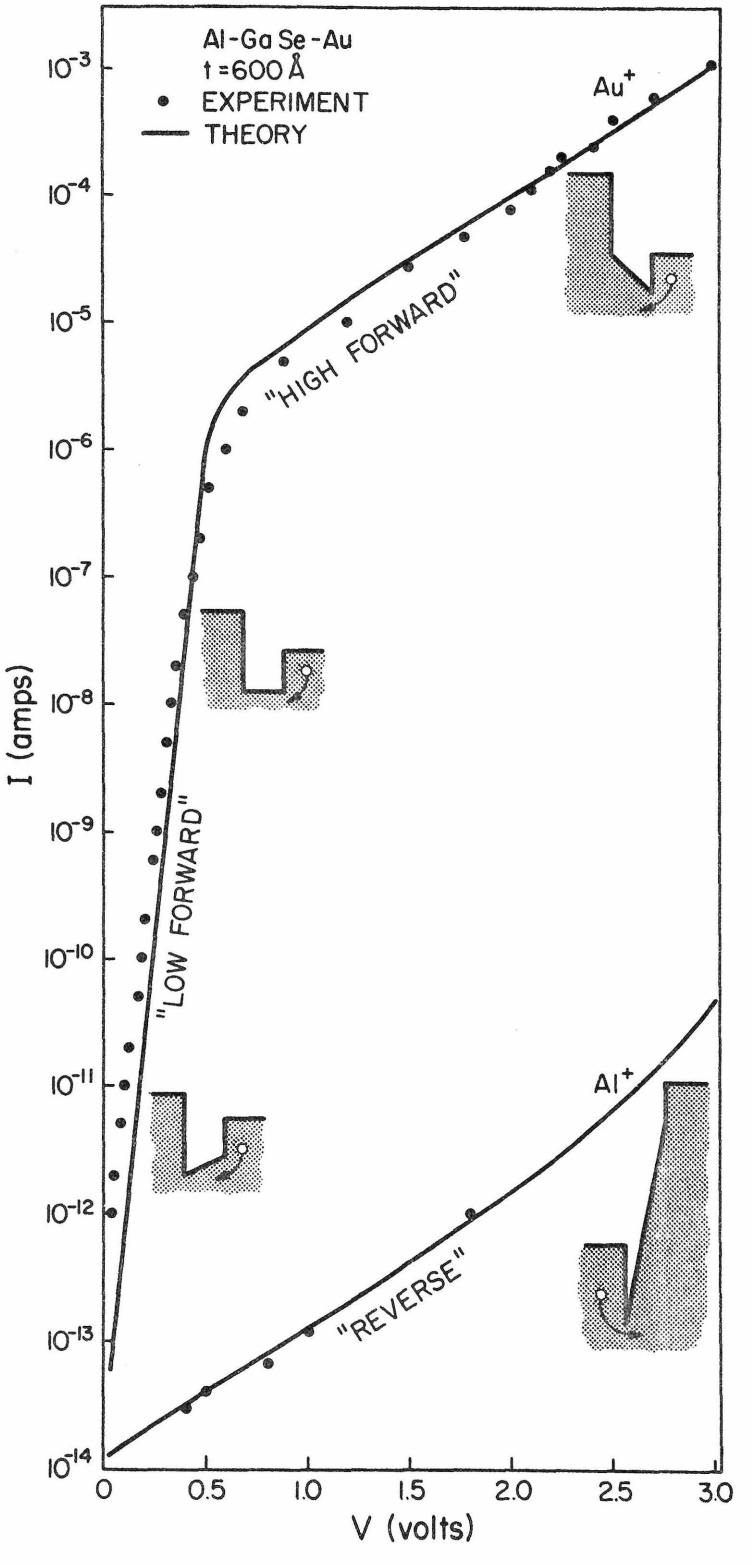
Al-Ga Se-Au
t=600 Å
EXPERIMENT
THEORY
Au+
"HIGH FORWARD"
"LOW FORWARD"
Al+
"REVERSE"
I (amps)
V (volts)
10-3
10-4
10-5
10-6
10-7
10-8
10-9
10-10
10-11
10-12
10-13
10-14
0
0.5
1.0
1.5
2.0
2.5
3.0

Fig. I.3

Fig. I.3 Current-voltage characteristic of an Al-GaSe-Au structure. Both directions of applied bias are shown on this figure. The dots are experimental data; the solid line is numerically calculated from the theory of thermionic contact-limited current (Eq. I.6-3) using parameters determined from prior experiments on bulk GaSe (no adjustable parameters were employed). Excellent agreement between theory and experiment is evident. The insets show partial band diagrams of the Al-GaSe-Au structure and illustrate the bias conditions we denote "low forward": $0 < V < (\phi_{Al} - \phi_{Au})$; "flat band": $V = (\phi_{Al} - \phi_{Au})$; "high forward": $V > (\phi_{Al} - \phi_{Au})$; and "reverse": $V < 0$. This descriptive notation is helpful when discussing thermionic contact-limited current flow because for a given structure it conveys a knowledge of the direction of current flow, the source metal, and the limiting barrier.

on applied bias since the limiting barrier (ϕ_{Al}-V) decreases linearly with voltage. In the absence of scattering and direct carrier tunneling, the slope of the log I vs. V curve is very nearly $\frac{1}{kT}$. High forward occurs when the applied bias is positive and greater than $\phi_{Al}-\phi_{Au}$. In this case the limiting barrier is ϕ_{Au}, and the source of the current carriers is the gold electrode. Image lowering of ϕ_{Au} and contributions to the current from thermal-field and field emission mechanisms cause the observed increases in current with increasing bias. Reverse occurs when the applied bias is negative. In this case the limiting barrier is ϕ_{Al}, and the source of the current carriers is the aluminum electrode. The increase in current with increasing bias observed in this case is a result of barrier lowering and tunneling, the same mechanisms which operate in the high forward.

The solid curves of Fig. I.3 are the theoretical current-voltage characteristic of an Al-GaSe-Au structure incorporating a 600Å single crystal film of GaSe. These curves were numerically calculated using the known properties of GaSe (see Section I.3) and a theoretical model (discussed below) of thermionic injection-limited currents adapted from the treatment by Murphy and Good[8,22] of the metal-vacuum interface.

In general, the expression for current as a function of applied voltage consists of the integral over all energies of two factors: a supply function which gives the flux of carriers from the source electrode, and a transmission function which gives the probability that a carrier incident on the limiting barrier is transmitted through it. In the approximation that the transmission function depends only on the

component of the carrier's energy normal to the metal-insulator interface and on the applied bias (via the electric field $\mathcal{E}$), the current may be written as

$$I(V) = e \int dE\ P(E_\perp,V)\ N(E_\perp,V) \qquad (I.6\text{-}3)$$

where $E_\perp$ is the component of the carrier energy which is perpendicular to the plane of the interface and V is the applied bias. $P(E_\perp,V)$ $N(E_\perp,V)$ are the transmission and supply functions, respectively. The limits on the integral in eqn. I.6-3 are such that all the contributions to the current are taken into account. Following Murphy and Good,[8] we assume that the metal may be described[23] by a single parabolic band with effective mass m_m^*. In this case the supply function is given by[24,25]

$$N(E,V) = \frac{4\pi m_m^*}{\beta h^3}\ A\ \ell n \left\{1+e^{-\beta[E-E_F(V)]}\right\} \qquad (I.6\text{-}4)$$

where A is the area of the sample, E_F is the Fermi energy of the metal supplying the carriers,[26] and $\beta = 1/kT$.

In determining the dependence of the transmission function on the perpendicular component of the energy two cases must be distinguished. In the first case, the carrier has a perpendicular energy which is greater than the maximum in the limiting barrier (eqn. I.6-2), and the transmission function (neglecting possible reflections at the interface[27]) is taken to be one. In the second case, the carrier has a perpendicular energy which is less than the maximum in the limiting barrier and must

tunnel through a portion of this barrier if it is to contribute to the current. If the behavior of the carrier for energies lying inside of the forbidden gap is adequately described by an effective mass m_i^*, then following the derivation of Murphy and Good[8]

$$P(E_\perp,V) = \left[-\frac{2}{3}\left(\frac{m_i^*}{\hbar^2}\right)^{\frac{1}{2}}\left(\frac{e}{\pi K_{opt}\epsilon_o}\right)^{\frac{3}{4}} \mathcal{E}^{-\frac{1}{4}} y^{-\frac{3}{2}} v(y)\right] \qquad \text{(I.6-5)}$$

where $y = (e\mathcal{E}/4\pi K_{opt}\epsilon_o)^{\frac{1}{2}}/(\phi_o - E_\perp)$. Physically, y is the ratio of the image lowering of the barrier energy to the difference between the perpendicular component of the carrier energy and the surface barrier energy ϕ_o. The function $v(y)$ is given by[28]

$$v(y) = 2^{-\frac{1}{2}}(1+a)^{\frac{1}{2}}\left\{\tilde{E}\left(\frac{2a}{1+a}\right)^{\frac{1}{2}} - (1-a)\tilde{K}\left(\frac{2a}{1+a}\right)^{\frac{1}{2}}\right\} \qquad \text{(I.6-6)}$$

where $a = \sqrt{1-y^2}$, and $\tilde{K}$ and $\tilde{E}$ are complete elliptic integrals of the first and second kind, respectively.

From the discussion of sections I.3, I.4 and I.5, we know that our experimental structures correspond to the energy band diagram of Fig. 2 and hence that the previous discussion of the ideal MIM structures is directly applicable. We therefore expect that experimental current-voltage characteristics should correspond to the results of theoretical calculations based on this band diagram. The theoretical current-voltage characteristic (solid line) appearing in Fig. I.3 has been calculated[29] for an Al-GaSe-Au structure 6.21×10^{-5} cm^2 in area and incorporating a GaSe film 600Å thick. The calculation is simply a numerical evaluation

of eqn. I.6-3 using the previously measured properties of bulk GaSe (see Section I.3). The solid black dots which also appear in Fig. 3 are data measured on a structure having a gold counterelectrode area 6.21×10^{-5} cm^2 and incorporating a 600Å thick GaSe film. (Film thickness is determined directly from the electrode area and a measurement of structure capacitance at zero bias: $t = K_{dc}\varepsilon_o A/C$). Excellent agreement between theory and experiment is evident from the figure. This agreement, in and of itself, gives strong support to the contact-limited transport model. Other predictions of this model must now be investigated.

C. Temperature Dependence

For external conditions such that both thermal-field emission and field emission are negligible the simple model of thermionic contact-limited current flow predicts that (at fixed applied bias) current should be exponentially dependent on temperature: $I \sim e^{-\phi_o/kT}$, where ϕ_o is the effective barrier energy limiting current flow. To confirm the thermionic origin of the currents observed in Al-GaSe-Au structures, it is necessary to experimentally check these predictions. Data obtained from such measurements are shown in Figs. I.4 and I.5. Values of applied bias were chosen such that current was limited either by the Al-GaSe barrier or by the Au-GaSe barrier.

From the inset of Fig. 4, it is clear that the slope of a line drawn through the data points should yield a value for the effective barrier height associated with the GaSe-Au interface. Evaluation of this experimental slope gives $\phi_o = 0.514$ eV which differs only slightly

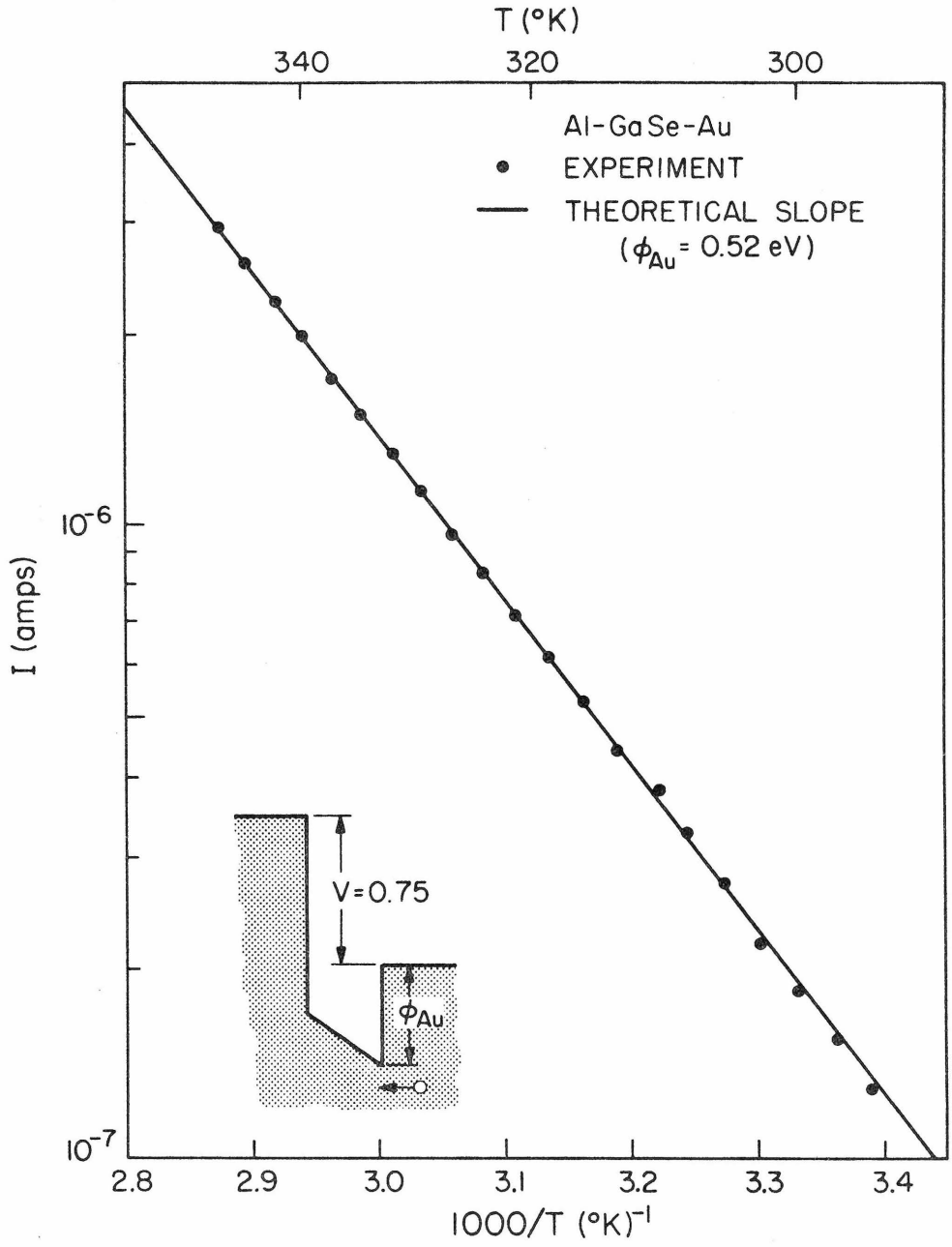

Fig. I.4 Current as a function of 1000/T for a V_{Au} = + 0.75 V (high forward) biased 600 Å thick Al-GaSe-Au structure. The dots are experimental data; the solid line is calculated by numerical evaluation of Eq. (I.6-3) as a function of temperature. The correspondence between theory and experiment confirms the thermionic nature of current flow at the Au-GaSe interface.

from the .52 eV value found by photoresponse experiments performed on bulk specimens. This slight deviation is due to lowering of the effective barrier which results from both the image-force and thermal-field emission. For larger biases (higher fields) this effective lowering becomes even larger.

From the inset to Fig. I.5, it is clear that the slope of the line of data points should yield a value for the effective barrier energy associated with the GaSe-Al interface. Evaluation of this slope gives ϕ_o = 1.02 eV, compared with the bulk photoresponse value of 1.05 eV. Image-force lowering (which is larger in this case than in the case discussed above because of the built-in field) accounts for a deviation of 0.046 eV.

For a comparison of observed behavior with detailed theoretical predictions, the solid lines plotted in both Fig. I.4 and Fig. I.5 were numerically computed directly from Eq. I.6-3. This calculation takes into account the entire distribution of carriers and hence the theoretical curves in Figs. I.4 and I.5 deviate slightly from the perfectly straight lines predicted by a purely thermionic model. As is evident from the figures, the agreement between theory and experiment is excellent. The correspondence between the barrier energies measured by photoemission experiments on bulk GaSe specimens and those measured thermally on MIM structures leaves no doubt concerning the thermionic origin of the observed currents, nor of their contact-limited nature.

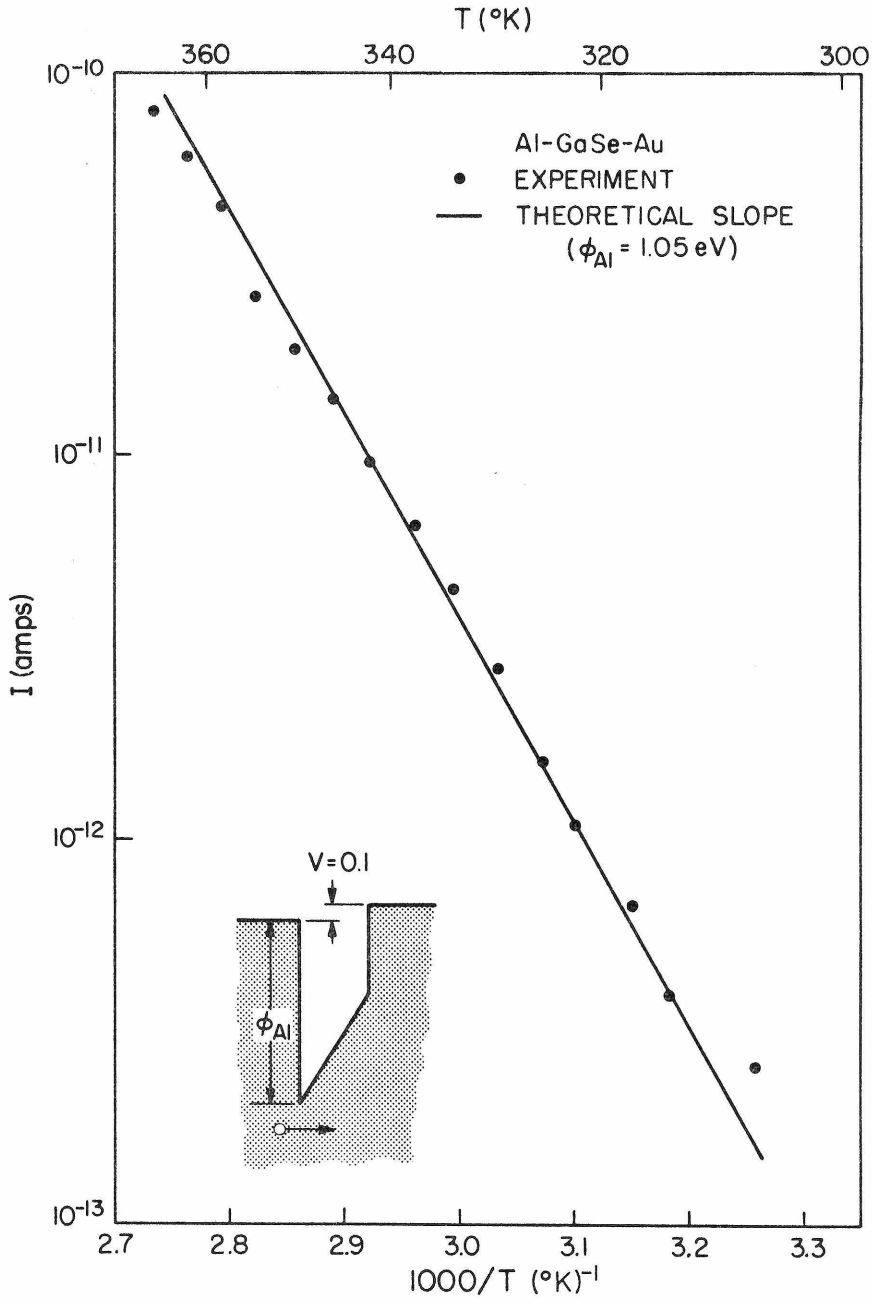

Fig. I.5 Current as a function of 1000/T for a V_{Al} = 0.1 V (reverse) biased 600 Å thick Al-GaSe-Au structure. The dots are experimental data; the solid line is calculated by numerical evaluation of Eq.(I.6-3) as a function of temperature. The correspondence between theory and experiment confirms the thermionic nature of current flow at the Al-GaSe interface.

I.7 BARRIER SHAPE AND CARRIER DISTRIBUTION

A. Photoresponse Measurements

The photoresponse technique[30] is perhaps the best method of determining interface barrier energies on bulk specimens. We have applied this technique to MIM structures to directly investigate the electric field dependence of the interface barrier energy. Results of this investigation unambiguously established the barrier potential to be in fact as deduced in Section I.6.

In the absence of appreciable tunneling,[31] photoresponse threshold (viz, ϕ_{photo}) is the energy difference between the Fermi level in the source metal and the maximum with respect to x of the barrier potential. Solving Eq. I.6-2 for its maximum yields

$$\phi_{photo} = \phi_o - \sqrt{\frac{e\mathcal{E}}{4\pi K_{opt}\,\varepsilon_o}} \qquad (I.7\text{-}1)$$

This result is the well-known Schottky lowering in which the effective interface barrier decreases as the square root of the total field $\mathcal{E}$.

Data obtained from photoresponse measurements performed on the same structure whose current-voltage characteristic appears in Fig. I.3 are presented in Fig. I.6. For a given applied bias, the barrier energy ϕ_{Al} was obtained from the intercept of a plot of the square root of photoresponse per incident photon as a function of photon energy.[30] The voltage dependence of ϕ_{Al} was obtained directly from the Al^+ voltage dependence of photoresponse at fixed photon

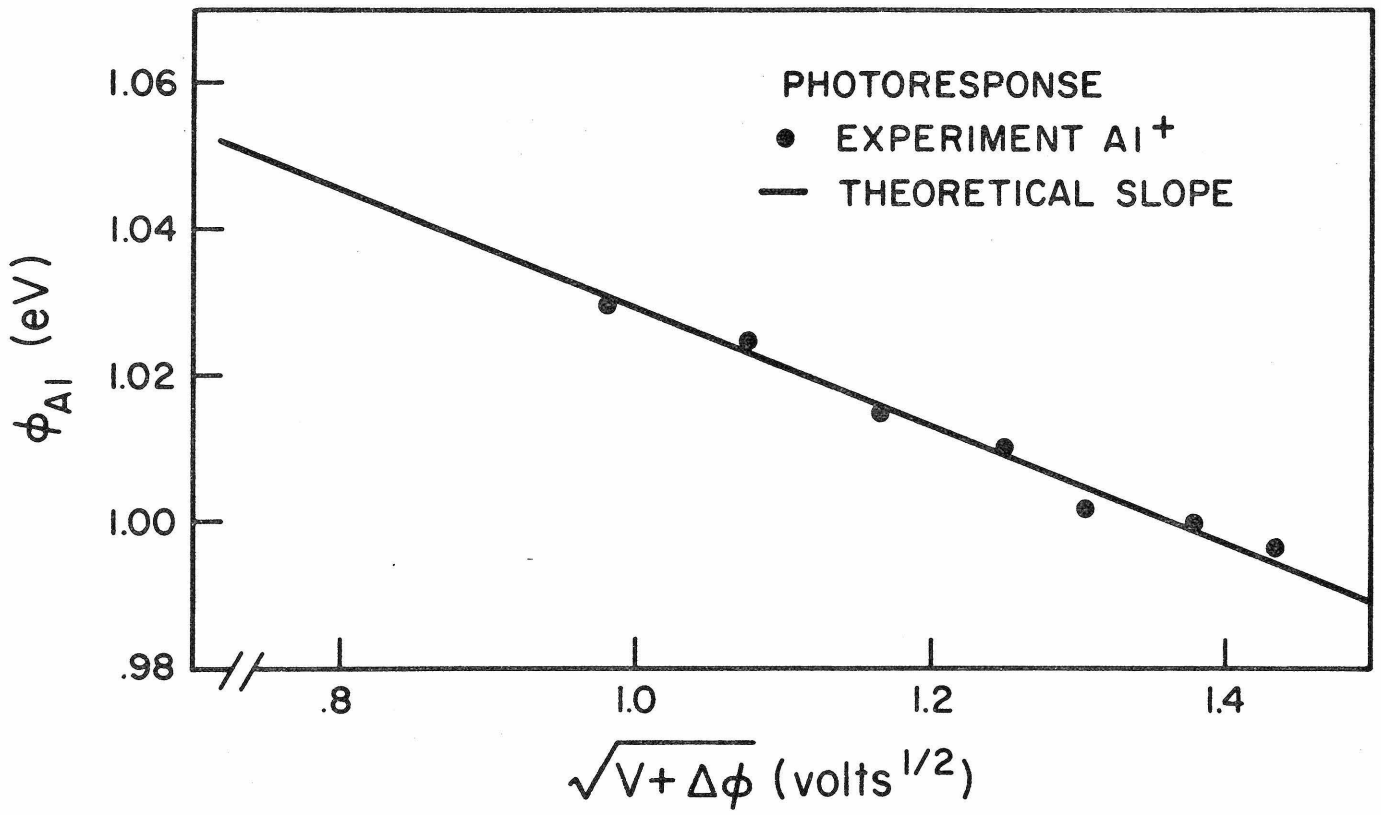

Fig. I.6 Dependence of the effective Al-GaSe barrier energy on applied bias. To facilitate comparison with theoretical predictions of Schottky lowering (see Eq. I.2-1) the barrier energy ϕ_{Al} is plotted vs. the square root of total internal bias: $V + (\phi_{Al} - \phi_{Au})$. The correspondence between theory and experiment confirms that the barrier energy exhibits Schottky lowering and is strong evidence that the barrier potential is, to good approximation, trapezoidal.

energy.[32] As shown in Fig. I.6, this barrier energy exhibits the Schottky lowering predicted by the image-force correction to the barrier potential.

B. Carrier Distributions

Having thus established that the actual barrier potential is well described by the simple Schottky model, we can use the contact-limited transport theory of Section I.6 to gain insight into the detailed mechanisms of current flow.

Results of detailed numerical calculations, specifically for the case of the 600 Å thick sample discussed above, are plotted in Fig. I.7. For each applied bias the solid curves illustrate the actual image-force lowered barrier potential; the dotted curve represents the (normalized) relative contribution per unit energy to the current of carriers with a given value of $E_\perp$. The extent to which any given carrier injection mechanism contributes to the observed current under a specific set of external conditions can be seen directly. As illustrated by this figure, the dominant mechanism of current transport shifts continuously, with increasing internal field, from thermionic emission to field emission. For reverse bias > 1.0 volt, a large portion of the current is contributed by carriers tunneling through the upper portion of the image-lowered barrier.

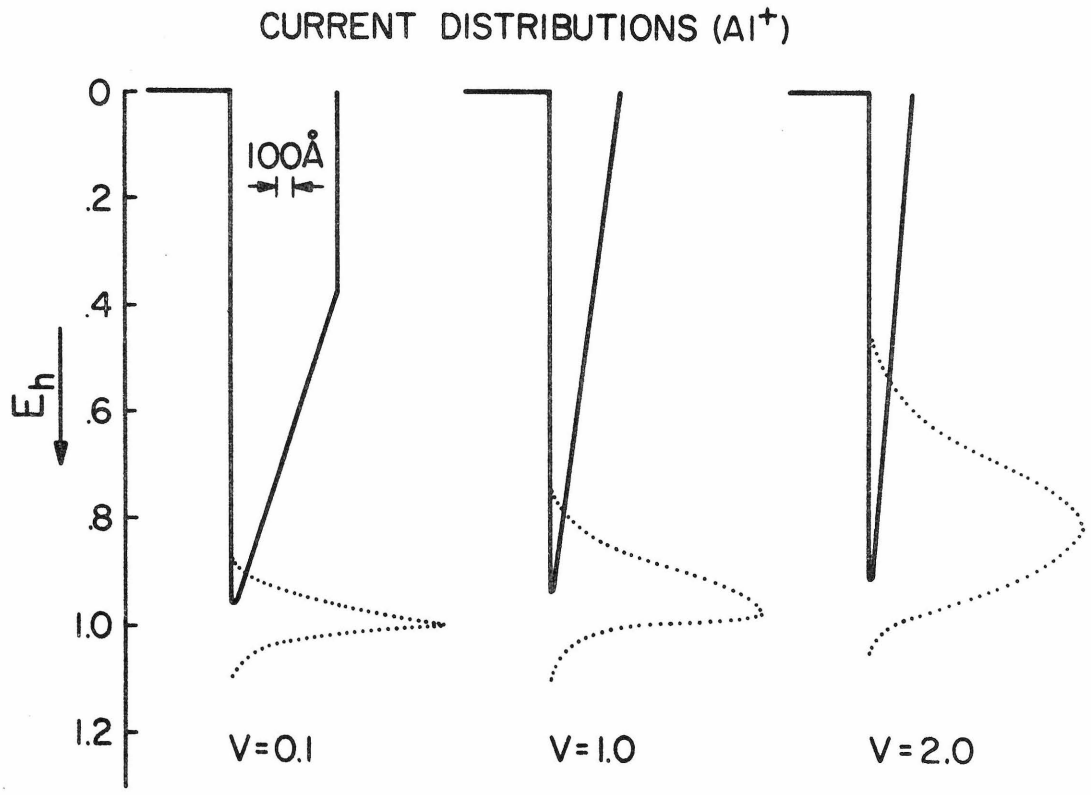

Fig. I.7 Theoretical (normalized) current distribution for a reverse biased 600 Å thick Al-GaSe-Au structure. The solid curves illustrate the shape of the image-force-lowered potential barrier; the dotted curves represent the distributions, as a function of hole energy E, of injected carriers. We note that the dominant injection mechanism shifts continuously with increasing bias from thermionic emission to thermally assisted tunneling. These curves have been calculated from the simple contact-limited current flow model discussed in the text. The validity of this model is assured by the previously discussed quantitative agreement between experiment and the predictions of this model.

I.8 CONCLUSION

Current flow in metal-insulator-metal structures is often very complex. In many cases physically distinct mechanisms can lead to qualitatively similar current-voltage characteristics. Interpretation of experimental observations is particularly difficult when the properties of the insulating layer are unknown. Hence, great care must be taken to avoid translating a lack of knowledge of the parameters of a structure into ambiguities about the physics of carrier transport. Many potential difficulties can be avoided if the parameters of an experimental structure are known from measurements which are independent of those performed to study current flow. With such a structure the physics governing current flow can be studied in detail because quantitative tests of the predictions of a given physical model are feasible.

In this study we have fabricated MIM structures containing single crystal films of the layer compound gallium selenide. Prior experiments on bulk specimens of single crystal gallium selenide provide data with which both the applicability and predictions of various models of current flow can be calculated. On the basis of such calculations we were able to deduce that space charge limitations would be unimportant and to anticipate thermionic, contact-limited currents. Extensive measurements performed on the MIM structures are in excellent quantitative agreement with these calculations. We therefore believe that this study provides the first unequivocal evidence for contact-limited current flow in solids.

I.A APPENDIX

Multiple image-force corrections to the barrier shape should be considered in a discussion of contact-limited current only if they significantly change the shape of the barrier potential near that contact which is limiting the current. For samples with insulating layers which are thick enough to rule out the possibility of a significant contribution to the total current from direct tunneling of carriers from one metal electrode to the other ($t \gtrsim 150$ Å), and for electric fields which are large enough to define one barrier as the limiting barrier, the influence of multiple images is quite small. To illustrate this point consider the deviation, $\Delta\phi(x)$, of the multiple image-force-corrected barrier potential from the single image-force-corrected barrier for x values near the limiting electrode. $\Delta\phi(x)$ is given by (See Eq. I.6-1)

$$\Delta\phi(x) = \frac{e}{8\pi K_{opt}\,\varepsilon_o t}\, f(d) = \frac{7.2\ \text{eV-Å}}{K_{opt}\, t}\, f(d) \qquad \text{(A-1)}$$

where

$$f(d) = \sum_{n=1}^{\infty} \frac{d^2}{n(n^2-d^2)} \qquad \text{(A-2)}$$

and $d = x/t$. In Fig. I.8 we have plotted $f(d)$ for d in the range 0 to 0.5 (for d greater than 0.5, we should correct the barrier shape for the image in the second electrode). This figure demonstrates that $f(d)$ is less than one throughout the range of d from 0 to 0.5.

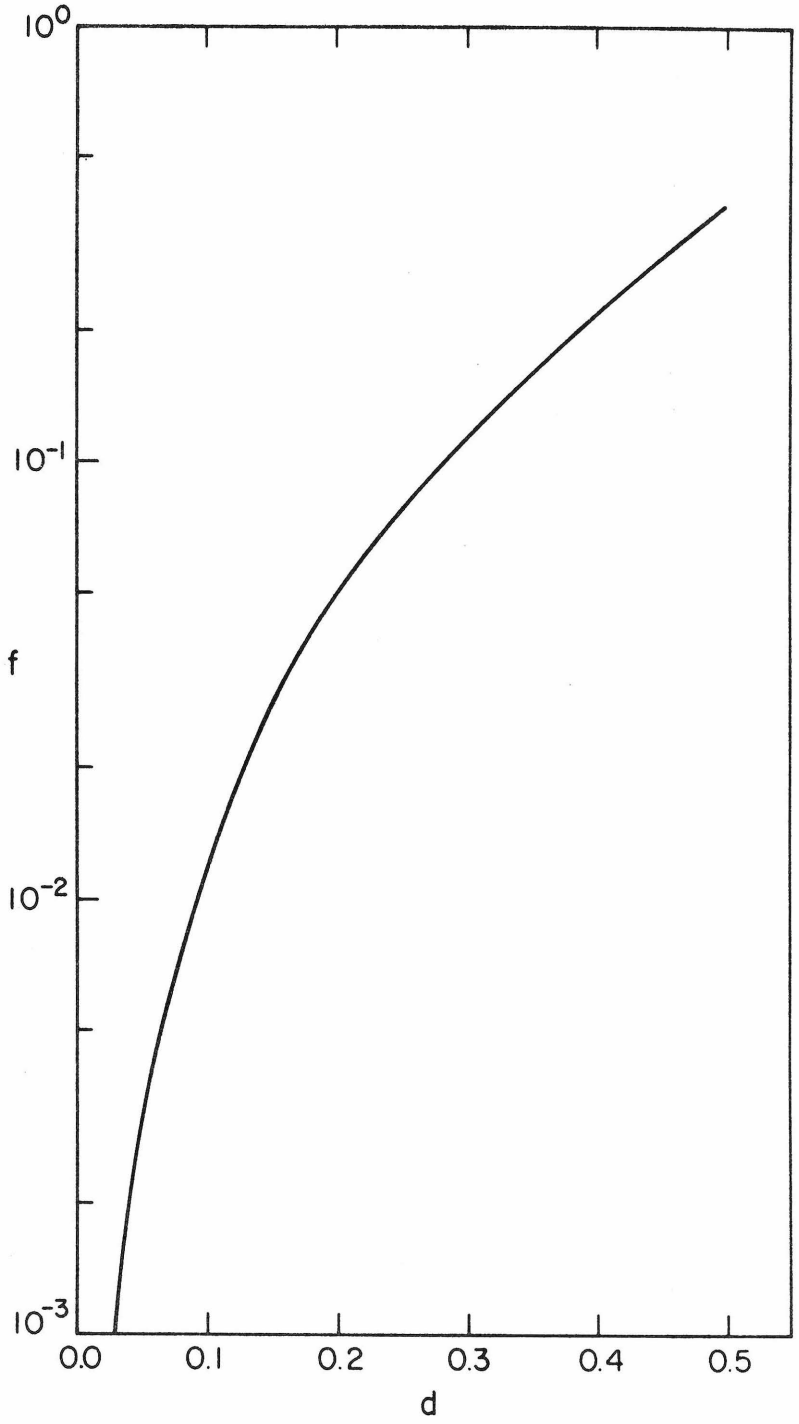

Fig. I.8 Dependence of the function f (see appendix) on the normalized distance d. This function measure the relative importance of the multiple image correction to the single image-force barrier lowering.

Thus, a crude upper bound for the contribution of multiple images to the barrier shape can be obtained by evaluating the numerical factor multiplying f(d) in Eq. A-1 for typical values of $K_{opt}(=7)$ and $t(= 200\ \mathring{A})$; this yields

$$\Delta\phi < 3.6 \times 10^{-3} eV \ . \qquad (A-3)$$

This estimate is very conservative. Values of d which are important in determining the current are frequently less than 0.5. Hence, a more appropriate bound of f(d) would be between 10^{-2} and 10^{-1}. We conclude that for all cases discussed herein, the effect of multiple image-force corrections to the barrier shape is negligible.

I.R REFERENCES

1. W. Schottky, Physik Z. 15, 872 (1914).
2. L. W. Nordheim, Proc. Roy. Soc. (London) A121, 626 (1928).
3. R. H. Fowler and L. W. Nordheim, Proc. Roy. Soc. (London) A119, 173 (1928).
4. A. Sommerfeld and H. Bethe, Handbuck der Physik, ed. by H. Geiger and K. Scheel (Verlug Julius Springer, Berlin, 1933), Vol. 24, No. 2.
5. E. Guth and J. C. Mullin, Phys. Rev. 61, 339 (1942).
6. W. W. Dolan and W. P. Dyke, Phys. Rev. 95, 327 (1954).
7. W. P. Dyke, J. P. Barbour, E. E. Martin, and J. K. Trolan, Phys. Rev. 99, 192 (1955).
8. E. L. Murphy and R. H. Good, Phys. Rev. 102, 1464 (1956).
9. P. R. Emtage and W. Tantraporn, Phys. Rev. Letters 8, 267 (1962).
10. C. A. Mead, Phys. Rev. 128, 2088 (1962).
11. J. J. O'Dwyer, J. Appl. Phys. 37, 599 (1966).
12. See for example: J. G. Simmons, Phys. Rev. Letters 15, 967 (1965); P. Mark and T. E. Hartman, J. Appl. Phys. 39, 2163 (1968).
13. H. Kamimura and K. Nahao, J. Phys. Soc. Japan 24, 1313 (1968).
14. P. C. Leung, G. Andermann, W. G. Spitzer, and C. A. Mead, J. Phys. Chem. Solids 27, 849 (1966).
15. P. Fielding, G. Fisher and E. Mooser, J. Phys. Chem. Solids 8, 434 (1959).
16. S. Kurtin and C. A. Mead, J. Phys. Chem. Solids 29, 1865 (1968).
17. G. Lewicki and C. A. Mead, Phys. Rev. Letters 16, 939 (1966).
18. See also: S. Kurtin, T. C. McGill and C. A. Mead, Phys. Rev. Lett. 25, 756 (1970).

19. Previous work indicates that surface barriers prepared on GaSe are not sensitive to whether the GaSe is cleaved in vacuum or in air (see Ref. 26).

20. All energies and potentials throughout this discussion are measured in eV. All other units are MKS.

21. The appendix defines criteria for neglecting the multiple image-force correction. For a detailed discussion of various approximations to the multiple image-force correction, see J. G. Simmons, J. Appl. Phys. 39, 1793 (1963).

22. Such adaptation has been previously discussed by several authors. See for example: W. Tantraporn, Solid State Electronics 7, 81 (1964). R. Stratton, Solid State Electronics 8, 175 (1965).

23. The question of what effective mass to use has been discussed by several authors. See for example: Ref. 21 and also C. Crowell, Solid State Electronics 8, 395 (1965). Since small deviations in the value of pre-exponential factors do not affect the qualitative character of the physics being studied we choose to use a conceptually simple model uncluttered by experimentaly indeterminate quantities.

24. R. Fowler and E. A. Gugenheim, Statistical Thermodynamics (Cambridge Press University Press, New York, 1952), p. 460.

25. In the low forward (see Fig. 13) carriers traverse the insulating region against the electric field before encountering the limiting barrier. Hence for the low forward, the assumed form of the supply function may be in error because both scattering of carriers within the insulator and reflection at the metal-insulator interface

have been neglected. These effects may be responsible for the slight deviation of calculated currents from those experimentally observed in the low forward.

26. The voltage dependence of the Fermi energy indicated in Eq. II.6-4 calls attention to the possible variation of this energy with respect to the energy zero as the applied bias is changed.

27. Recently some authors have addressed themselves to the problem of correcting for reflections at the metal-semiconductor interface (in Schottky barrier diodes). See for example C. R. Crowell and S. M. Sze, J. Appl. Phys. 37, 2683 (1966); C. R. Crowell, Solid State Electronics 8, 395 (1965), Solid State Electronics 12, 55 (1969). However, since reflection leads only to a change in the pre-factor multiplying the current, experimental attempts to verify the modification due to reflection have proven to be exceedingly difficult.

28. R. E. Burgess and K. Kroemer, Phys. Rev. 90, 515 (1953).

29. The effective mass of electrons in either metal is taken to be one throughout these calculations.

30. C. A. Mead, Solid State Electronics 9, 1023 (1966), and the references contained therein.

31. The role of tunneling near the top of the image-force lowered potential barrier may be assessed by computation of the quantum mechanical transmission coefficient as a function of energy (referenced to ϕ_{photo}). As long as the energy range over which a significant number of the incident carriers can tunnel through the barrier is small compared with the energy range over which photo-

response measurements are made, the primary effect of tunneling will be to contribute a "tail" to the photoresponse data. If this tail is ignored, the barrier energy measured by photoresponse will be ϕ_{photo}.

32. F. A. Padovani, Rev. Sci. Instr. 39, 772 (1968).

PART II

TUNNELING CURRENTS

II.1 INTRODUCTION

Although the basic concepts of tunneling are firmly rooted in the early quantum mechanics[1], only recently has progress been made in gaining a quantitative understanding of tunneling in solids[2]. Perhaps the greatest impediment has been the experimental problems associated with the fabrication of suitable structures.

Since the probability amplitude of a tunneling electron is exponentially damped in space[3], the "forbidden" region through which tunneling is to occur must be extremely thin (<100Å) to favor tunneling over other current flow mechanisms. It has not in general been possible to cleave single crystal solids into films this thin and hence other techniques of fabricating a thin forbidden region are traditionally employed. Perhaps the best known technique is the controlled oxidation[3] of a metal, followed by vacuum deposition of counter-electrodes thus forming metal-insulator-metal structures. Early studies[5,6,7] of direct inter-electrode tunneling in solids were conducted using structures fabricated by this or similar techniques. It was observed that currents flowing in such structures were often temperature independent and exhibited a nearly ohmic dependence on applied voltage for small applied voltages. This sort of behavior is in qualitative agreement with the predictions of simple tunneling theory. However, when attempts were made to obtain quantitative agreement between theory and experiment, perplexing discrepancies arose.

The theoretical model first applied to tunneling in MIM structures[8] dealt explicitly with a symmetric barrier potential; the forbidden region within this potential was assumed to behave like a vacuum (except for a dielectric constant different from unity). In many cases the gross differences between theory and experiment could be minimized by using an "effective thickness" for the insulating film or an "effective mass" for the tunneling electron. These parameters were chosen specifically to bring theory and experiment into agreement, could not be independently determined, and bore little relation to the actual parameters of the structure under study. Although this approach served as a convenient method for classifying experimental data, it did not provide a deep understanding of tunneling, or even unequivocal evidence that tunneling was indeed being observed.

Of course, it was realized that the chemical composition of the grown insulating film was not uniform, and that the metal-oxide interface was in all likelihood far from the idealized rectangular barrier shape usually assumed. In fact, non-symmetric current-voltage curves were often observed for nominally symmetric structures (e.g. Al-Al_2O_3-Al). The extent to which these difficulties invalidated the model was not clear, and hence fundamental inadequacies in the model went unnoticed. A large stride toward overcoming the major experimental difficulties was taken by McColl *et al*[9] in the study of thin mica films cleaved from bulk crystals. Despite crystal-to-crystal variation, great consistency was observed in all measurement obtained on structures fabricated from a given initial bulk crystal. Parameters required to describe tunneling currents in thin mica films were in good agreement

with the corresponding independently measured properties of the bulk mica. Yet, certain problems remained including an apparent systematic deviation between theory and experiment. Careful analysis of the data indicated that characterizing the quantum mechanically forbidden region as a simple vacuum was probably a misleading over-simplification.

A successful approach toward the resolution of this theoretical/experimental problem was taken by Lewicki et al[10,11] who studied current flow in thin amorphous films of aluminum nitride (formed by plasma discharge nitriding). Working with Stratton[12], they recognized the importance of the E-k dispersion relation within the forbidden gap in describing tunneling through solids, and were able to piece together an E-k relation for AlN by measuring the thickness dependence of the tunneling probability at several values of applied bias. This experimentally determined E-k relation successfully describes many of the tunneling phenomena observed in AlN thin films.

In this paper we report a synthesis and extension of the previously described techniques. By choosing to study thin films of the layer compound gallium selenide we can fabricate nearly ideal structures. All of the parameters relevant to current flow in these structures can be determined by independent experiments. The thin gallium selenide film under study is single crystal in character and therefore has the properties of bulk material, and also well-defined interfaces. An improved analytical technique for determining the energy-momentum dispersion relation within the forbidden gap of a solid (from appropriate current-voltage measurements) is discussed and applied to data obtained from metal-Ga-Se-metal structures. The re-

sulting E-k relation is shown to be an intrinsic property of GaSe. Tunneling currents in GaSe can thus be quantitatively understood in terms of this E-k relation, the independently determined parameters of a given structure, and a simple model of current flow via tunneling.

II.2 THEORY OF TUNNELING IN METAL-INSULATOR-METAL STRUCTURES

Current flow arising from the direct tunneling of electrons from one metallic electrode to another through an intervening insulating layer provides a unique opportunity to study the quantum mechanical interaction of electrons with solids. A tunneling electron interacts continuously with the solid through which transport is occurring; the details of this interaction can be unravelled only if a great deal of information about the experimental structure is available. Ideally, one seeks sufficient independent information about an experimental structure to construct an accurate (and hopefully simple) energy band representation. The potential barrier through which tunneling is occurring should be well-defined and experimentally controllable. Having satisfied these criteria, a straightforward model of tunneling can be constructed with some assurance that it is a reasonable representation of the physical situation. In the discussion that follows, we presume (and will in fact demonstrate in Section II.3) that these criteria are fulfilled for the metal-GaSe-metal structures discussed here, and that a simple trapezoidal barrier potential is appropriate.

Discussions of tunneling are often based upon the transfer Hamiltonian model[13,14]. In this description an idealized tunneling structure, as schematically illustrated in Fig. II.1, is divided into three separate regions. For electrons with energies of interest, two of the regions are allowed (electrodes); the third region is unallowed (insulator). Current flow arises when there is a net transfer of electrons from one electrode to the other due to the interaction of the

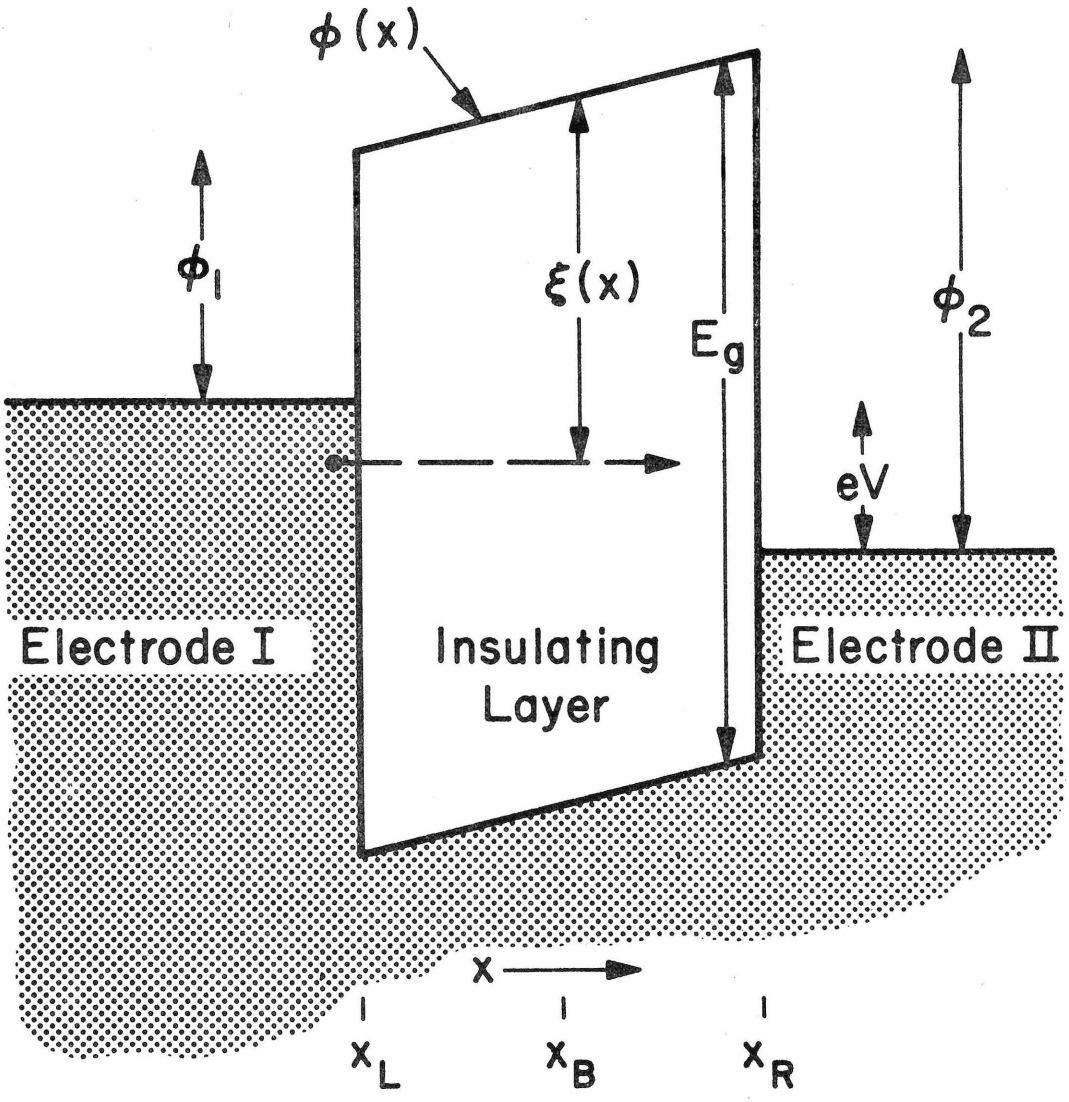

Fig. II.1 Schematic energy band representation of an ideal metal-insulator-metal tunneling structure in which electrode II is biased V volts with respect to electrode I. ϕ_1, ϕ_2 are metal-insulator barrier energies; $\phi(X)$ is the (trapezoidal) barrier potential; $\xi(X)$ is the energy of an electron tunneling from electrode I to electrode II, referenced to $\phi(X)$; the spatial coordinate X is used both as a continuous variable and to denote distinct regions of the structure

two electrodes through the insulator. This system is described by the quantum mechanical Hamiltonian

$$H = H_L + H_R + H_T \tag{II.2-1}$$

where H_L is the Hamiltonian for the left electrode (see Fig. II.1), H_R is the Hamiltonian for the right electrode and H_T (transfer Hamiltonian) contains the interaction between the two electrodes due to the insulating region. The transfer Hamiltonian may be expressed simply in terms of basis states $\{|\alpha>\}$ and $\{|\beta>\}$. The set $\{|\alpha>\}$ is the set of single particle solutions of the Hamiltonian for the left electrode and the insulating layer which carry current toward the insulating layer. The set $\{|\beta>\}$ is a similar set of functions for the right electrode. Using this basis, H_T is given by the expression

$$H_T = \sum_{\alpha,\beta} \left(M_{\alpha\beta}\ C_\alpha^\dagger\ C_\beta + M_{\alpha\beta}^*\ C_\beta^\dagger\ C_\alpha \right) \tag{II.2-2}$$

where $M_{\alpha\beta} = i\hbar\, J_{\alpha\beta}(X_B)$ and $J_{\alpha\beta}(x_B)$ is the matrix element of the current operator between the states α and β integrated over a plane parallel to the metal-insulator interface at some position, X_B, in the insulating layer[13]. That is,

$$J_{\alpha\beta}(X_B) = \int_S \underset{\sim}{dS} \cdot \underset{\sim}{J}_{\alpha\beta}(X_B), \tag{II.2-3}$$

where

$\underset{\sim}{J}_{\alpha\beta}(X_B) = \langle\alpha|\underset{\sim}{J}(X_B)|\beta\rangle$ and S is the plane described above.

Application of Fermi's Golden Rule to compute the net rate of transfer produced by H_T gives

$$I(V) = 2\pi e\hbar \sum_{\alpha\ \beta} |J_{\alpha\beta}|^2 \left\{ f_L(\varepsilon_\alpha) - f_R(\varepsilon_\beta) \right\}, \qquad \text{(II.2-4)}$$

where $I(V)$ is the current from left to right for an applied bias V; f_L and f_R are the Fermi factors for the left and right electrode, respectively; and ε_α and ε_β and the single particle energies of the state α and the state β, respectively. In deriving equation II.2-4 it is assumed that the electrodes are adequately described by a single particle formalism.

Evaluation of the matrix element $J_{\alpha\beta}$ for direct tunneling in the standard way (see, for example, references 15,16,17) yields an expression for the current density

$$j(V) = \frac{2e}{h}\int dE \int \frac{d^2k_{\|}}{(2\pi)^2}\, g(E,k_{\|})[f_L(E) - f_R(E)]\exp\left\{-2\int_{X_L}^{X_R} k(E,k_{\|},X)\,dX\right\}, \qquad \text{(II.2-5)}$$

where $\underset{\sim}{k}_{\|}$ is the parallel component of the wave vector of the electron in the electrode. It is important to note that the exponential factor

which dominates this expression results from the exponential decay of the electronic wavefunction in the forbidden insulating region: $k(E,k_{||},X)$ is the attenuation constant. For single crystal insulators k may be thought of, in band structure terms, as the imaginary part of the complex wave vector[18,19] within the forbidden gap. In general, k is a function of the electron energy, E; the parallel component of the wave vector, $k_{||}$; and position in the insulator, X. The dependence on X is due to the applied potential and interface potentials which change the features of the band structure of the insulator relative to the electron's energy.

In Eq. II.2-5, $g(E,k_{||})$ is a pre-exponential factor which results from the matching of the wavefunctions at the interfaces. Its exact theoretical form will depend on the assumed boundary conditions. Attempts at experimentally verifying the form of $g(E,k_{||})$ from structure in the bias dependence of the tunneling current have failed[15]. Since k, the function of interest, is insensitive to the exact form or value of $g(E,k_{||})$ we will take it to be unity. This approximation is supported by calculations on several simple models which all yield $g \simeq 1$.

Further simplification of Eq. II.2-5 can be realized by noting the rapid variation of the exponential factor with $k_{||}$. This allows us to use the saddle point method to obtain a useful approximation for the integral. Taking the dependence of $k(E,k_{||},X)$ on $k_{||}^2$ to be given by

$$k(E,k_{||},X) = \sqrt{k^2(E,0,X) + k_{||}^2} \qquad \text{(II.2-6)}$$

we have

$$j(V) = \frac{\frac{e}{2\pi h}\int dE\ \exp\left\{-2\int_{X_L}^{X_R} k(E,0,X)dx\right\}}{\int_{X_L}^{X_R}\frac{dx}{k(E,0,X)}}\left[f_L(E)-f_R(E)\right] \quad \text{(II.2-7)}$$

Since most tunneling experiments are performed at low temperature (to minimize thermionic currents) it is often a good approximation, and always theoretically handy, to take the temperature to be zero. This approximation makes sense if the natural width of the energy distribution of tunneling electrons is appreciably greater than the width added by the thermal tail on the Fermi distribution in the source electrode.[20]

There remains one useful simplification of II.2-7 to be discussed. The energy E may be related to the spatial coordinate X such that k becomes a function of a single variable $\xi(X)$. This new variable $\xi(X)$ is the difference in energy between the conduction band and the energy of an electron located at X:

$$\xi(X) = \phi(X) - E \ . \quad \text{(II.2-8)}$$

Re-expressing $j(V)$ in terms of $\xi(X)$

$$j(V) = \frac{\frac{e}{2\pi h}\int dE\ \exp\left\{-2\int_{\xi(X_L)}^{\xi(X_R)} \frac{d\xi}{d\phi/dX}\,k(\xi)\right\}}{\int_{\xi(X_L)}^{\xi(X_R)} \frac{d\xi}{(d\phi/dX)k(\xi)}} \qquad \text{(II.2-9)}$$

This expression, although somewhat approximate, is of adequate precision and contains the basic physics of tunneling. A quantitative interpretation of experimental data using this expression requires $\phi(X)$ [and hence $\xi(X)$] be known independent of the measurement of tunneling currents.

Assuming now the trapezoidal barrier potential[21] as shown in Fig. II.1

$$\phi(X) = \phi_1 + (\phi_2 - \phi_1 - V)X/t, \qquad \text{(II.2-10)}$$

and for an applied bias[22] in the range $-\phi_1 < V < \phi_2$, Eq. II.2-9 becomes

$$j(V) = \frac{\frac{e}{2\pi h}\int_0^V dE\ \exp\left\{\frac{-2t}{\phi_2-\phi_1-V}\int_{\phi_1+E}^{\phi_2+E-V} d\xi\ k(\xi)\right\}}{\int_{\phi_1+E}^{\phi_2+E-V} \frac{d\xi\ \ t}{(\phi_2-\phi_1-V)k(\xi)}} \qquad \text{(II.2-11)}$$

This equation is a suitable basis for interpreting tunneling currents in structures known to have a trapezoidal barrier shape.

To interpret tunneling I-V characteristics in terms of $k(\xi)$ (i.e., the dispersion relation for the imaginary part of the wave vector) Eq. II.2-11 must be solved for $k(\xi)$ given $J(V)$ and the other parameters in the equation. For certain values of barrier energy and applied voltage, and for certain $k(\xi)$ functions, the distribution in energy of the tunneling electrons can be accurately approximated by a single sharp peak. In this case expression II.2-11 reduces to the familiar simple form[12] used by Stratton et al, and the interpretation may be accomplished by simple mathematical manipulations. However, in general, Eq. II.2-12 must be solved without simplifying approximations. Thus, one is faced with solving a nonlinear integral equation of the Volterra type of the first kind. Numerical solution is unavoidable.

Equations of the type given in Eq. II.2-11 are usually solved by an adaptation of the well-known Newton's method for obtaining the roots of a system of nonlinear equations[23]. Basically, this technique consists of making an initial guess and then computing corrections to this guess from the integral equation. In detail, let

$$\mathcal{L}\{j_{exp}(V),k(\xi)\} = j_{exp}(V) - \frac{\frac{e}{2\pi h}\int_0^V dE\ \exp\left\{-\frac{2t}{(\phi_2-\phi_1-V)}\int_{\phi_1+E}^{\phi_2+E-V} k(\xi)\ d\xi\right\}}{\int_{\phi_1+E}^{\phi_2+E-V} \frac{d\xi}{k(\xi)}\ \frac{t}{(\phi_2-\phi_1-V)}} \qquad \text{(II.2-12)}$$

where $j_{exp}(V)$ is the experimental current density as a function of bias and $\mathcal{L}$ is a function of both $j_{exp}(V)$ and $k(\xi)$. Obviously, $\mathcal{L}$ will be identically zero when a solution is attained. Let $k_o(\xi)$ be the function which makes $\mathcal{L} \equiv 0$, that is, $k_o(\xi)$ is the solution. In general, $k_o(\xi)$ is unknown. However, some initial guess at $k_o(\xi)$ is made. This guess $k(\xi)$, is related to $k_o(\xi)$ by an equation

$$k(\xi) = k_o(\xi) - \delta k(\xi) \tag{II.2-13}$$

where $\delta k(\xi)$ is the correction required to make $k(\xi)$ equal $k_o(\xi)$. Substituting II.2-13 into Eq. II.2-12 and expanding in a Taylor's series about $k(\xi)$, we have

$$0 = \mathcal{L}\{j_{exp}(V),k(\xi)\} + \int \frac{\delta}{\delta k(\xi)} \mathcal{L}\{j_{exp}(V),k(\xi)\}\, \delta k(\xi)\, d\xi + \ldots \tag{II.2-14}$$

where $\delta \mathcal{L}/\delta k(\xi)$ is the functional derivative of $\mathcal{L}$ with respect to $k(\xi)$. Neglecting higher order terms in Eq. II.2-14, this equation gives a value of $\delta k(\xi)$

$$\delta k(\xi) = -\int dV \frac{\delta}{\delta k(\xi)} \mathcal{L}^{-1}\{j_{exp}(V),k(\xi)\}\, \mathcal{L}\{j_{exp}(V),k(\xi)\} \tag{II.2-15}$$

where $\delta \mathcal{L}^{-1}/\delta k(\xi)$ if it exists is the inverse of the integral operator appearing in Eq. II.2-14. Existence of the inverse determines that range of $j_{exp}(V)$ which is required to specify $\delta k(\xi)$ and $k_o(\xi)$ over a specific range of ξ. This point will be discussed in more detail below.

Evaluation of $\delta\mathcal{L}/\delta k(\xi)$ may be accomplished by substituting $k(\xi) + \delta k(\xi)$ for $k(\xi)$ in Eq. II.2-12 and expanding in $\delta k(\xi)$. The term linear in $\delta k(\xi)$ gives $\delta\mathcal{L}/\delta k(\xi)$. The result of such a calculation is shown in Fig. II.2 where the explicit dependence of $\delta\mathcal{L}/\delta k(\xi)$ on V and ξ is shown. If the array in Fig. II.2 is evaluated on a mesh in V and ξ with equal number of points in ξ and V (as is done in the numerical solution of II.2-13), then one obtains a square matrix. If this matrix has a determinant which is different from zero, then the finite set of numerical equations which replace II.2-13 has a unique solution. This condition determines the range of V which will give a unique set of values of k_o on the mesh of ξ. Thus, it is possible to test the uniqueness of the calculated solution by computing the inverse of this matrix. While this method does not provide a rigorous mathematical test for uniqueness, it does suffice for the problem at hand.

Numerical solution proceeds in a straightforward manner[17,24]. Some difficulty is encountered in solving the linear Eq. II.2-13 as a result of numerical instabilities. These difficulties may be overcome by the use of a powerful technique recently developed by Franklin for converting an ill-posed linear problem into a well-posed stochastic problem[25].

$$\frac{\delta \mathcal{L}}{\delta K(\xi)} = \int_{\alpha}^{\beta} \Gamma \, dE$$

$$\Gamma(V,\xi,E) = \frac{e}{2\pi h \zeta}\left[2 - \frac{(\phi_2-\phi_1-V)}{t}\left(\frac{1}{k^2(\xi)\,\zeta}\right)\right] \exp\left\{\frac{-2t}{\phi_2-\phi_1-V}\int_{\phi_1+E}^{\phi_2+E-V} k(\xi')\,d\xi'\right\}$$

$$\zeta = \int_{\phi_1+E}^{\phi_2+E-V_1} \frac{d\xi'}{k(\xi')}$$

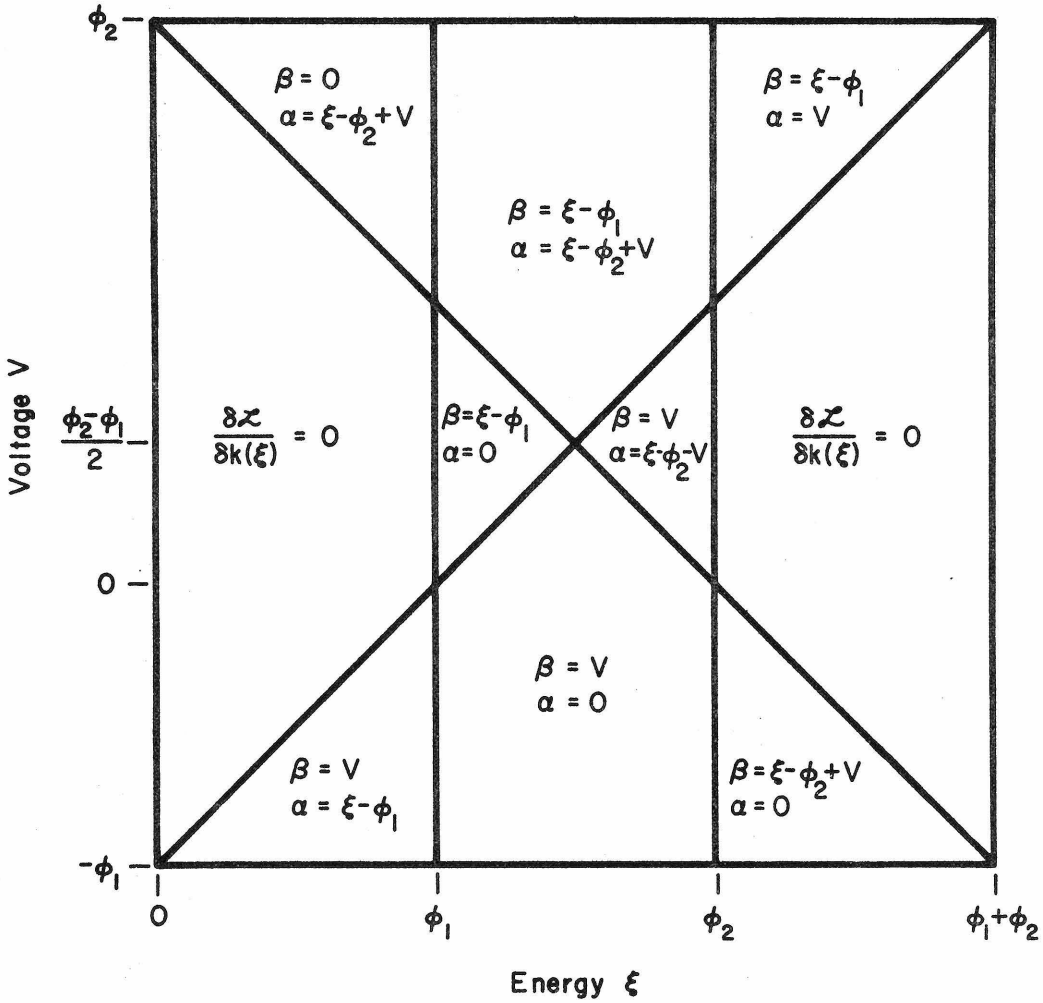

Fig. II.2 The functional derivative $d\mathcal{L}/dk(\xi)$, used in the calculation of the energy-momentum dispersion relation from appropriate experimental current-voltage data, is shown along with a diagram of the plane in voltage-energy space over which this functional derivative is to be evaluated.

II.3 EXPERIMENTAL CONSIDERATIONS

A. Gallium Selenide

Ideally one would like to take a well characterized bulk insulator, cleave it into thin section (100 Å thick), and incorporate these thin sections into MIM structures. Such an approach is not usually feasible for a variety of practical reasons. There does exist, however, a family of solids (the layer compounds) which is well suited to this approach.

Layer compounds are distinguished by their unusual crystallographic structure. Each layer (typically several atoms thick) is strongly bonded internally but only weakly bonded to its neighbors. Hence, thin single crystal films can be obtained by pulling or peeling a macro single crystal apart. This technique for fabricating well-defined MIM structures was pioneered by Foote and Kazan[26] and used by McColl in his study of current flow in thin films of mica.

Gallium selenide[27] is the particular layer semiconductor chosen for this study. GaSe was chosen because it is easy to work with, large single crystals can be easily grown by the modified Bridgeman technique, and prior experiments have well characterized the properties of bulk specimens. In Part I the advantages of utilizing GaSe for the fabrication of thin MIM structures have been confirmed. That study provided an excellent example of contact-limited thermionic current flow. The quantitative agreement between theory and experiment which was observed is good evidence that the bulk and interface properties

of GaSe are sufficiently well known to make a tunneling study worthwhile. Listed below are those properties[27,28] of our "as grown" GaSe specimen which are relevant to tunneling currents in thin film structures:

Band gap	$E_g = 2.0eV$
Low frequency dielectric constant	$\epsilon_o = 8$
Optical dielectric constant	$\epsilon_{opt} = 7$
Al-GaSe interface barrier energy	$\phi_{Al} = 1.08eV$
Au-GaSe interface barrier energy	$\phi_{Au} = 0.52eV$
Cu-GaSe interface barrier energy	$\phi_{Cu} = 0.68eV$
Trap density	$N_t < 10^{14}/cm^3$
Carrier density at 300^oK	$p \sim 3 \times 10^{14}/cm^3$

B. Fabrication of MIM Structures

The technique by which MIM structures containing thin films of GaSe are fabricated is straightforward, but worthy of mention. Single crystal films of GaSe, perhaps 10μ thick, are peeled from a large boule and electroded on one side by vacuum evaporating aluminum from a tungsten filament at a residual pressure of 10^{-7} torr. Aluminum is chosen because it adheres well to the rather inert GaSe surface. The GaSe flakes are then bonded with 100% solids, silver loaded epoxy to a brass block of convenient dimensions. The exposed surface of the GaSe film is thereafter peeled away by successive application and removal of Scotch Transparent Tape (3M #810). Care is taken that a continuous film of GaSe is removed at each peel to avoid possible contamination of the GaSe surface with adhesive from the tape. As the film thins, interference colors become visible. With continued peeling, the film becomes too thin to generate interference colors. At this juncture it is, of course, not at all clear to the experimenter that any film remains. The specimen is then again placed in the vacuum system and gold or copper counter-electrode evaporated onto the freshly exposed GaSe surface. A fine wire mesh is used to define a regular array of square dots, 4.5×10^{-3} cm^2 in area, as counter-electrodes. The specimen is now complete and ready for preliminary testing to determine if it contains MIM structures of appropriate and uniform thickness.

C. Preliminary Calculations

The properties of the single crystal GaSe film incorporated within metal-GaSe-metal structures are known, and hence the shape of the potential barrier presented by this insulating film may be calculated. If image force barrier lowering and space charge within the GaSe film may be neglected, the barrier potential will be trapezoidal:

$$\phi(X) = \phi_1 - \left(\frac{\phi_1 - \phi_2 - eV}{t}\right) \qquad \text{(II.3-1)}$$

Space charge distorts the potential barrier shape because field lines originate or terminate on the trapped charge. Using the worst case assumption that all traps are ionized, integration of Poisson's equation yields $\Delta V = eN_t t^2/2\varepsilon < 10^{-3}$ which is totally negligible.

Carriers in transit induce image charges in the metallic electrodes. The attraction between a charge in transit and its images modifies the barrier potential. The extent to which this modification is significant can be estimated from the leading term in the complete (infinite series) multiple image force correction.

$$\Delta\phi = \frac{e}{16\pi\varepsilon X} - \frac{e}{8\pi\varepsilon t}\sum_{n=1}^{\infty}\frac{X^2}{n[(nt)^2 - X^2]} \qquad \text{(II.3-2)}$$

The magnitude of this correction depends on the choice of dielectric constant. Since a tunneling electron interacts with the barrier during

its entire passage, tunneling is, as indicated by the magnitude of the RC tunneling time, a slow process; atoms within the insulating layer have sufficient time to react to the passing charge and hence the low frequency dielectric constant is appropriate[21]. Using the value of ε_o for GaSe, it follows that the image force correction to the barrier shape amounts to a lowering of the barrier by less than 30 millivolts and a narrowing of less than one Å. These corrections are within the experimental error of our measurements, and may be neglected.[29]

Being now assured that the actual potential barrier within metal-GaSe-metal structures is well approximated by the simple trapezoidal model, an estimate of the conditions under which direct interelectrode tunneling is likely to be the dominant mechanism of current flow can be made. Bulk limitations have been shown[28] to be negligible even for 600Å films and hence can be neglected here. Thermionic currents have an exponential dependence on barrier height and temperature[28]

$$J_{TH} = J_o \, e^{-\phi/k_B T} \qquad \text{(II.3-3)}$$

where $J_o \sim 120T^2$ amp/cm^2 and k_B is Boltzman's constant. Tunneling probability (and hence tunneling current) increases exponentially with decreasing tunneling path length[10]

$$J_T = J_o' \, e^{-2kt} \qquad \text{(II.3-4)}$$

where $\hbar^2k^2/2m^* = E$ (parabolic band approximation) and $J_o' = (e/8\pi h)(\phi/t^2) \simeq 1.5 \times 10^{-6}\ \phi[eV]/t^2[cm^2]$ amp/eV. Assuming $\phi \simeq .6eV$, and $t \simeq 10^{-6}$ cm, $J_o' \simeq 10^2$ amps/cm^2. Tunneling will be the dominant mechanism of current flow if $J_T > J_{TH}$ i.e.

$$J_o\, e^{-2kt} >> J_o\, e^{-\phi/k_BT} \qquad \text{(II.3-5)}$$

This expression is a condition on both t and T. Since the thickness dependence of the tunneling probability is its most striking feature, it is worthwhile working at as low a temperature as possible, thus extending the thickness range over which tunneling is the dominant current flow mechanism. The lowest barrier with which we are concerned is $\phi_{Au} \simeq 0.5eV$. Taking $k \simeq 0.4\text{Å}^{-1}$ ($E = 1/2eV$, $m^* = 1$) as a rough estimate, tunneling is thus expected to dominate for $t << 100\text{Å}$ at 77^oK and for $t << 30\text{Å}$ at 300^oK.

D. Measurement Technique

An important experimental question is the temperature at which current-voltage measurements are to be made. Room ambient is most convenient but the interface barrier energies in GaSe structures are sufficiently low that thermionic currents are expected to be dominant except in extremely thin structures, thus unduly restricting the thickness range over which measurements can be taken. Liquid helium temperatures are ideal for eliminating thermionic currents, but the inability to temperature cycle GaSe MIM structures without mechanically destroying them, and the need to sample many structures to assure reliable data, make working in this temperature range extremely difficult.

As a workable compromise between the limitations of ambient and liquid helium environments, a measurement technique for use at liquid nitrogen temperature was evolved. The specimen bearing substrate is entirely immersed in liquid nitrogen after fabrication, and remains immersed through the entire measurement process. Viewing of the specimens to locate suitable individual structures for probing (with a fine gold wire) and measurement is accomplished with a specially constructed "under nitrogen viewer." This viewer[30] is an evacuated thin walled stainless steel conical tube fitted with sapphire windows at either end. The thermal conductivity of this viewer is sufficiently small that one end can be immersed under the surface of a liquid nitrogen bath, and permit viewing of objects therein, without excessive bubbling or boil-off and without frosting at the exposed end. With this viewer a given specimen could be probed for a period of several hours, and many structures investigated. Care was taken to choose a fine, springy probe wire with a rounded tip to avoid mechanically damaging the structure under test.

E. Selection of Structures

Preliminary measurements consist of determining the capacitance of each MIM structure on a given substrate to ascertain which structures have insulator thickness within the interesting (<100Å) range. Questions of insulator uniformity, the validity of the trapezoidal barrier approximation, and the dominance of tunneling as mechanism of current flow must be answered before detailed analysis is undertaken. These questions are coupled and may be simply resolved. Assuming the simple trapezoidal barrier model (Fig. II.1) with an arbitrary E-k relation in the forbidden gap of the insulator, the simple ideas of an exponentially damped wavefunction lead to a tunneling probability which decreases exponentially with increasing tunneling path[3]. Near zero bias the tunneling probability is inversely proportional to the tunneling time RC and is given by[10]

$$RC = \frac{\epsilon h}{2\pi e} \frac{m_\perp}{m_\parallel} \frac{1}{\bar{k}(\xi)} \exp\left[2t\bar{k}(\xi)\right] \qquad \text{(II.3-6)}$$

where $m_\parallel$ is the electronic effective mass parallel to the direction of current flow, and $m_\perp$ the electronic effective mass perpendicular to current flow. Hence, near zero bias the natural logarithm of RC should depend linearly on insulator thickness t with proportionality constant $2\bar{k}(\xi)$ and where $\bar{k}(\xi)$ is the average value of k encountered in the tunneling path corresponding to an incident electron with zero transverse momentum and energy equal to the metal Fermi energy. Therefore, experimental observation of a zero bias tunneling time which is

exponentially proportional to insulator thickness t is a good evidence that tunneling is the dominant mechanism of current flow and that the trapezoidal barrier model is appropriate.[31]

In addition to a tunneling time experimentally proportional to insulator-thickness, the zero thickness intercept of this plot should be within an order of magnitude of $\varepsilon h/2\pi e(1/\overline{k}) \simeq 8 \times 10^{-15}$ sec. Major deviations from this value require further investigation. Having thus identified (by simple measurements performed on the structure under study) tunneling through a trapezoidal barrier as the mechanism of current flow, this technqiue can be refined and used to select uniform thickness structures from the multitude incorporating an insulating film of non-uniform thickness (i.e. those having cleavage steps).

Consider the physical situation. The experimental specimens consist of nominally 5 to 20 layers of GaSe. A cleavage step of one or more layers will drastically affect the spatial distribution of current under a given counter-electrode, since current flow via tunneling is exponentially weighted toward thinner films. However, the apparent thickness, as determined from capacitance measurements, is weighted only linearly by thickness variations. Hence, for every apparent thickness it is possible to observe RC time constants substantially below that corresponding to a uniform insulator thickness. Clearly, a specimen selection technique is required to prevent a morass of confusing and self-contradictory data from being subjected to detailed analysis. The technqiue is simple. One merely selects those samples bounding the experimental half-plane of ℓn RC vs t measurements. A large number of specimens must be examined, but if tunneling is

indeed the mechanism of current flow, a well-defined bounding line will eventually emerge[32]. If this line is indeed straight, and its intercept of the expected magnitude, then the trapezoidal barrier assumption may be assumed valid (particularly if calculations of the expected barrier shape using the known parameters of the bulk material from which thin film structures are fabricated predict this simple barrier shape, as is the case for metal-GaSe-metal structures).

II.4 RESULTS AND INTERPRETATION

A. Al-GaSe-Au Structures

Fig. II.3 shows the zero bias time constant of a selection of Al-GaSe-Au structures plotted vs apparent GaSe thickness (as determined from capacitance measurements). The data shown were obtained from those specimens of highest resistance and hence of most nearly uniform insulator thickness. These data form a straight line over a wide thickness range, and hence direct tunneling through a trapezoidal barrier is indicated as the dominant mechanism of current flow. The slope of this straight line gives a good estimate of $\overline{k}(\xi)$ as indicated by Eq. II.3-6. The error bar shown on one data point is representative of the error in apparent thickness arising from scatter in the actual area of individual counter-electrodes as formed in the specimen fabrication process. This random error is the most important uncertainty in this series of experiments since the thickness enters calculated currents in the exponent.

Fig. II.4 presents detailed current-voltage data obtained on structures of uniform thickness (selected according to the procedure discussed in the previous section; see also Fig. II.3). Data were obtained over that voltage range, for each bias direction, for which direct inter-electrode tunneling is possible. This voltage range ($V < \phi_1$, $V < \phi_2$; see insert to Fig. II.4) is know a priori since the metal-GaSe interface barrier energies are known from prior experiments on bulk specimens. The data of Fig. II.4 (solid symbols) correspond to structures ranging from 57Å to 97Å in insulator thickness.

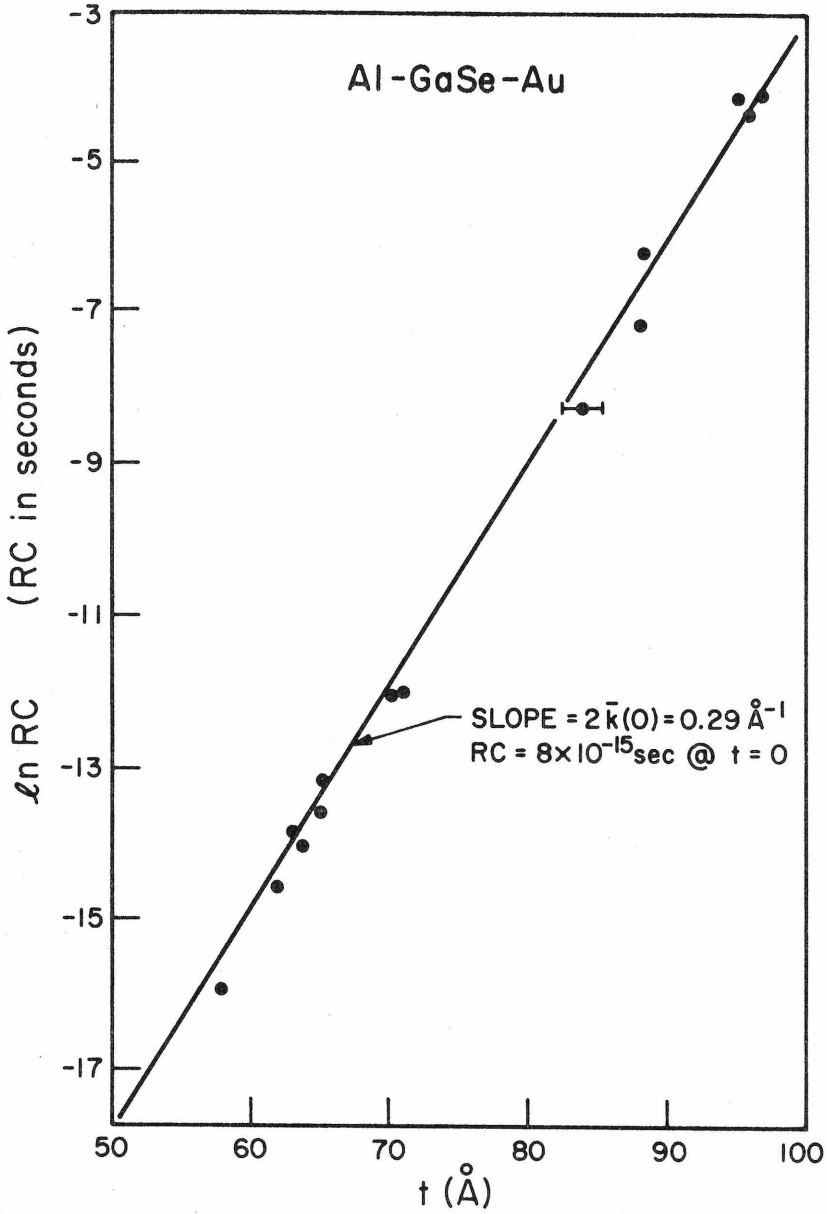

Fig. II.3 A plot of ℓn RC (measured near zero bias) vs apparent thickness t (as calculated from measured structure capacitance). Only data for those structures with the largest experimentally observed RC time constant are shown for each apparent thickness. These data correspond to structures having the most nearly uniform insulating layers, as explained in the text. Since a straight line is a good fit to the data, direct inter-electrode tunneling is indicated as the dominant conduction mechanism. The typical error bar, shown on one data point, corresponds to the area scatter in counter-electrode area, as measured photographically.

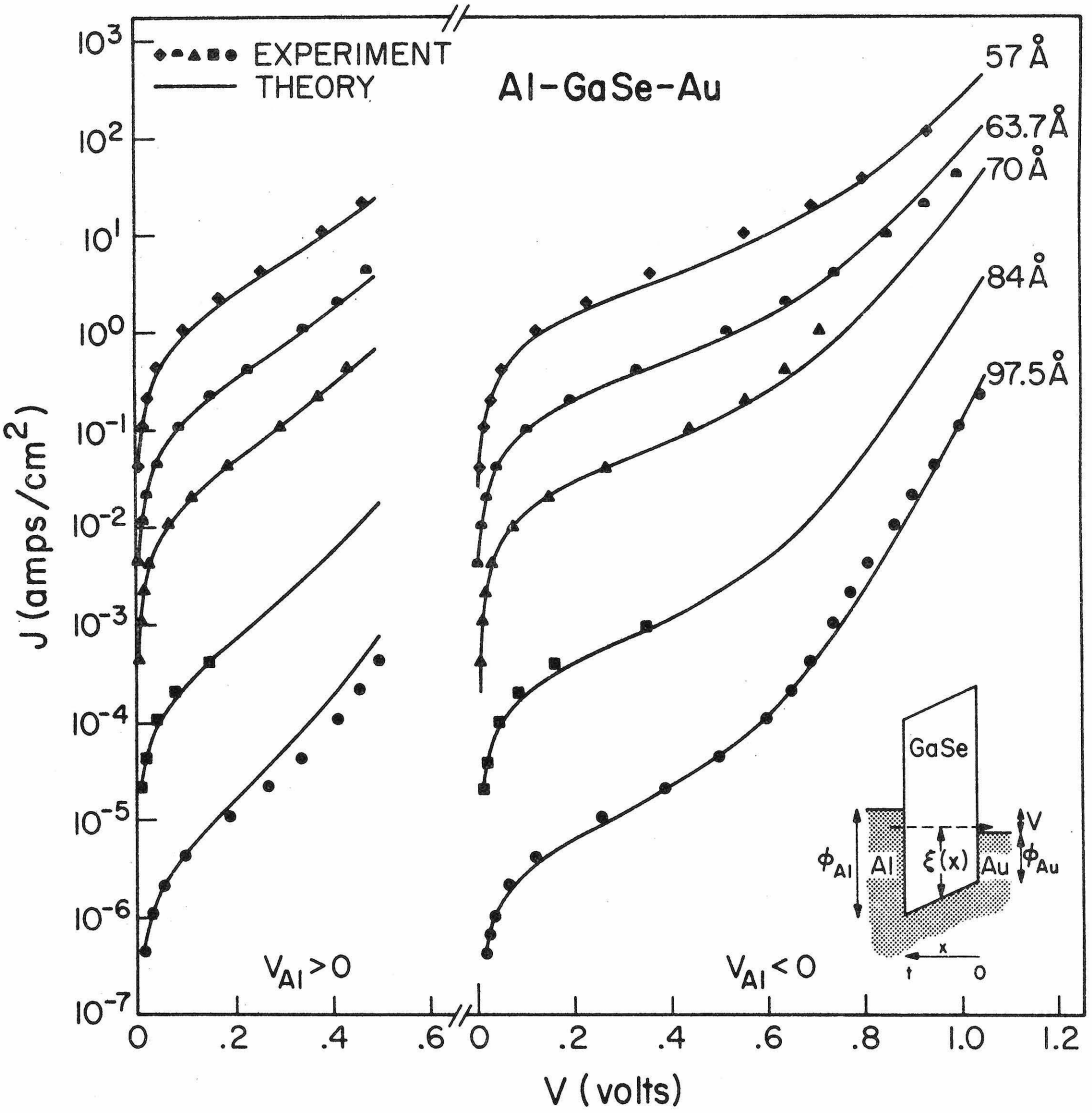

Fig. II.4 Current-voltage curves, for both directions of applied bias, of a number of Al-GaSe-Au structures. Solid symbols represent experimental data obtained on structures whose apparent thickness was calculated directly from the measured structure capacitance. Theoretical curves (solid lines) were calculated from the E-k relation of Fig. II.5, the known properties of GaSe, and the tunneling model of Section II.2 (Eq. II.2-11). Agreement between theory and experiment is seen to be very good. The inset to this figure shows the schematic energy bond representation of Al-GaSe-Au structures.

The data in Fig. II.4 were used as input to the numerical inversion program discussed in Section II.2 to obtain approximate E-k curves for GaSe. Inversion of the I-V curve for each thickness yields an E-k curve. These E-k curves were extremely similar and hence were averaged to obtain an overall best-fit E-k curve, shown in Fig. II.5. This energy-momentum dispersion relation is parabolic near the valence band, as expected, and departs from parabolicity toward mid-gap. The implications of this E-k curve are discussed below, after its accuracy has been established.

The theoretical I-V curves in Fig. II.4 were calculated directly from the E-k curve of Fig. II.5, the known parameters of GaSe (Section II.3), and the simple tunneling theory of Section II.2 as represented by Eq. II.2-11. The exceptionally good agreement between theory and experiment as illustrated by Fig. II.4 is evidence that the model of Section II.2 is adequate to describe tunneling in Al-GaSe-Au structures, since the E-k curve is highly over-specified by the data. That is, each I-V curve contains enough information to uniquely define the E-k relation over the relevant portion of the forbidden gap. The observation of quantitative agreement between current-voltage curves measured for a wide range of insulator thickness, and theoretical predictions based on a single E-k relation, indicates a complete self-consistency of the theoretical model with the experimental situation. As a consequence, we are well assured at this point that direct inter-electrode tunneling is the dominant mechanism of current flow in Al-GaSe-Au structures and that a single E-k dispersion relation accurately describes the tunneling phenomenon over a wide range

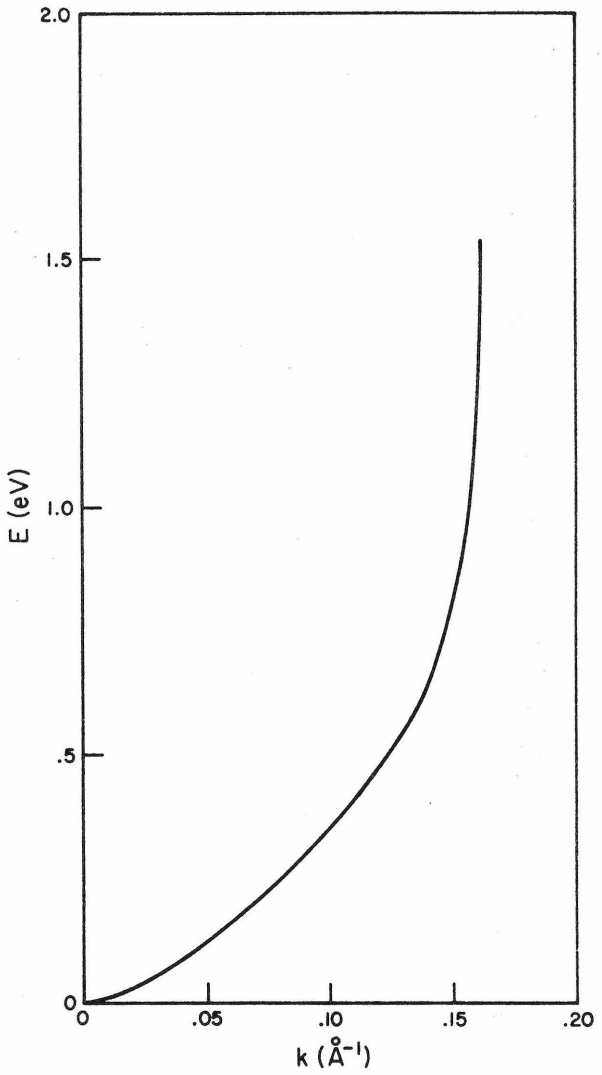

Fig. II.5 The experimentally determined energy-momentum dispersion relation within the forbidden gap of GaSe. This relation is an average of the E-k relations determined by numerically inverting each experimental I-V curve of Fig. II.4. Since only that portion of the E-k relation from the valence band up to $\phi_1 + \phi_2$ is active in determining the tunneling currents within a given MIM structure, the use of aluminum and gold as electrodes limits the range over which E(k) may be calculated to that shown (i.e., $\phi_{Al}+\phi_{Au}\simeq 1.5$ eV). This relation is parabolic near the valence band, as expected, but possesses rather little curvature for E>0.6 eV.

of insulator thickness. Further experiments are required to assure that the E-k relation thus far obtained is an intrinsic and fundamental property of GaSe.

B. The E-k Dispersion Relation

A crucial test of the validity (as indeed a fundamental and accurately determined property of GaSe) of the E-k relation of Fig. II.5 is the quantitative prediction of tunneling currents in structures other than the Al-GaSe-Au ones from which this relation was determined. For example, a tunneling electron in a Cu-GaSe-Au structure encounters a range of k for each applied bias which is quite different from that in an Al-GaSe-Au structure. As may be seen in the inset of Fig. II.6 the band diagram of a Cu-GaSe-Au structure is distinguished from that of an Al-GaSe-Au structure by the 0.4eV lower Cu-GaSe barrier energy.

The known properties of GaSe in conjunction with the E-k relation of Fig. II.5 are, as previously discussed, adequate to permit calculation of the tunneling current-voltage curves to be expected in Cu-GaSe-Au structures. The result of such a calculation (as per Section II.2 - with no adjustable parameters of any sort) is shown in Fig. II.6 along with data obtained on an experimental structure. The thickness used in this calculation is (as throughout this paper) determined directly from the measured capacitance of the experimental structure. The agreement between theory and experiment, shown in Fig. II.6, is excellent evidence that the E-k relation previously determined for GaSe is a fundamental and intrinsic property of GaSe.

The accuracy to which the energy-momentum dispersion relation of GaSe has been determined in this series of experiments may also be gauged by the comparison, presented in Fig. II.7, between the experimentally determined E-k curve and a common analytic approximation

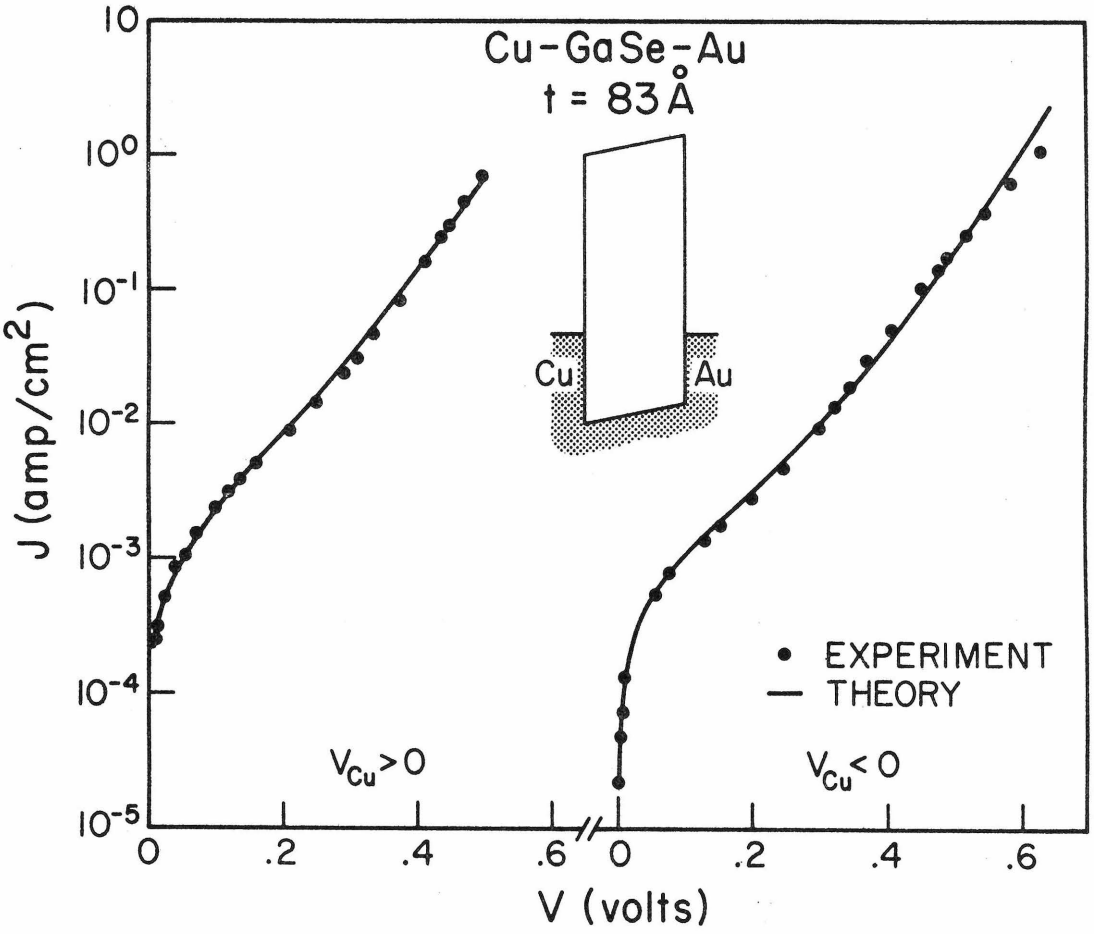

Fig. II.6 The experimental current-voltage curve of an 83 Å (as determined directly from the measured capacitance) Cu-GaSe-Au structure is shown by the solid symbols. The solid curve is calculated from the E-k relation of Fig. II.5, the known properties of GaSe, and the tunneling model of Section II.2 (Eq. II.2-11)). Agreement between theory and experiment is excellent thereby indicating that the previously determined E-k relation is intrinsic to GaSe. The inset shows a schematic energy band representation of the Cu-GaSe-Au structure.

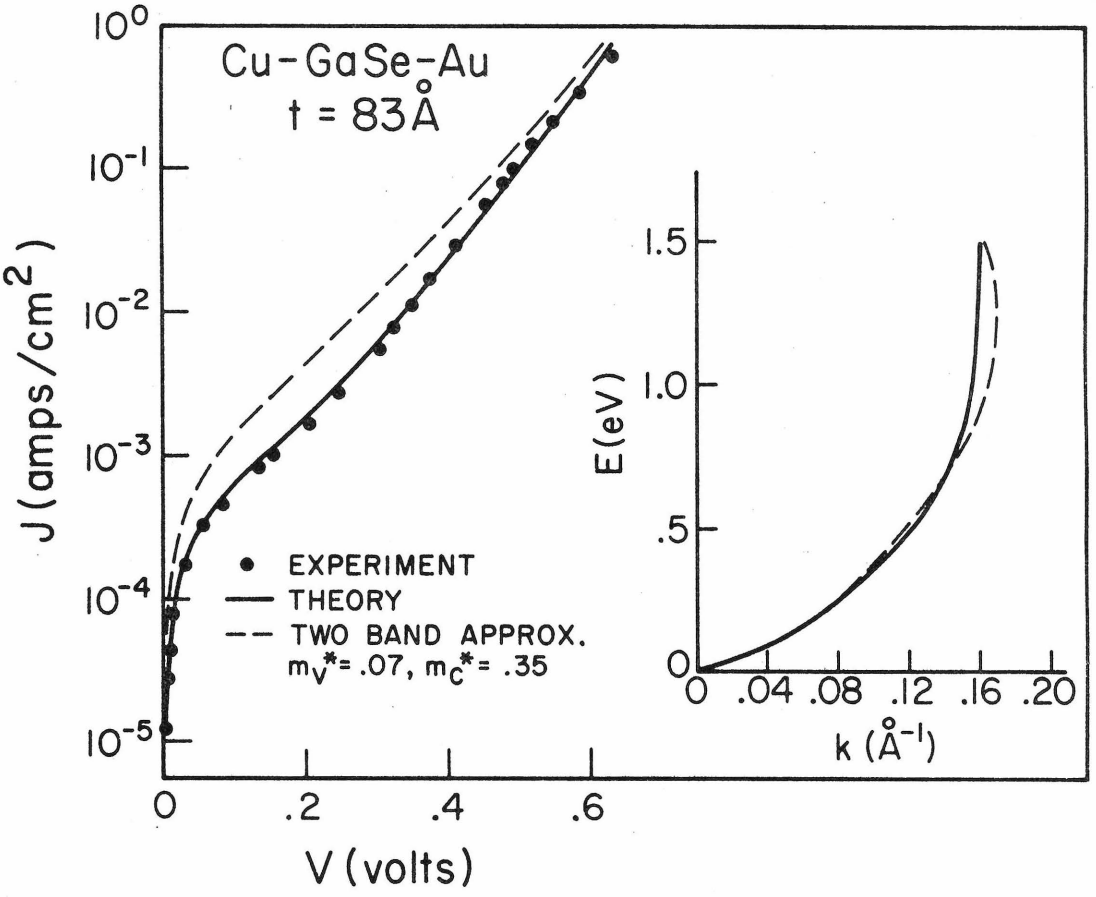

Fig. II.7 This figure presents both the experimentally determined E-k relation of GaSe and also a common two parameter approximation (Franz's two band model), and compares the tunneling currents predicted by each. The sensitivity of the I-V curve to small changes in the E-k relation may be gauged by comparison of the deviation between the two E(k) curves and the corresponding J(V) curves.

(Franz's two band model: $m_v^* = 0.07$, $m_c^* = 0.35$). The inset shows that the experimentally determined E-k relation (solid line) and the two band approximation differ only slightly. Yet the experimental I-V curve (solid circles) is seen to be in distinctly better agreement with the predictions of the actual E-k curve than with those of the approximation.

C. Energy Distribution of Tunneling Electrons

Having at our disposal an accurate E-k relation, the physics of electron tunneling may be more fully appreciated by using the previously discussed techniques to numerically calculate the energy distributions of tunneling electrons.

Energy distributions of tunneling electrons are shown for several values of applied bias in Fig. II.8. These distributions have been calculated for Al-GaSe-Au structures having thicknesses at the extremes of the range studied; the calculations span the range of biases over which direct inter-electrode tunneling is possible. For reference, a band diagram is shown for each bias condition. The number beneath each distribution (shaded curve) is the relative magnitude (i.e. scaling factor) of the peak of that distribution. Each distribution is drawn on a linear scale so that a visual estimate of its width will be meaningful.

Considering first the thicker (97Å) structure, it is clear that the nearly flat part of the E-k curve (see Fig. II.5, $E > 0.6$eV) leads to rather broad tunneling electron distributions at low bias. However, as the bias is increased the relevant portion of the E-k curve is extended toward $E = 0$ and hence the tunneling distribution becomes very peaked about the source electrode Fermi level. This peaking is exactly what is expected because the exponential damping of the electronic wavefunction heavily weights the transmitted distribution toward small values of k. At small insulator thicknesses, however, the weighting toward low k is correspondingly less. Therefore, in thin structures electrons at all possible energies contribute to the tunneling current, even at high bias. The degree to which this contribution is

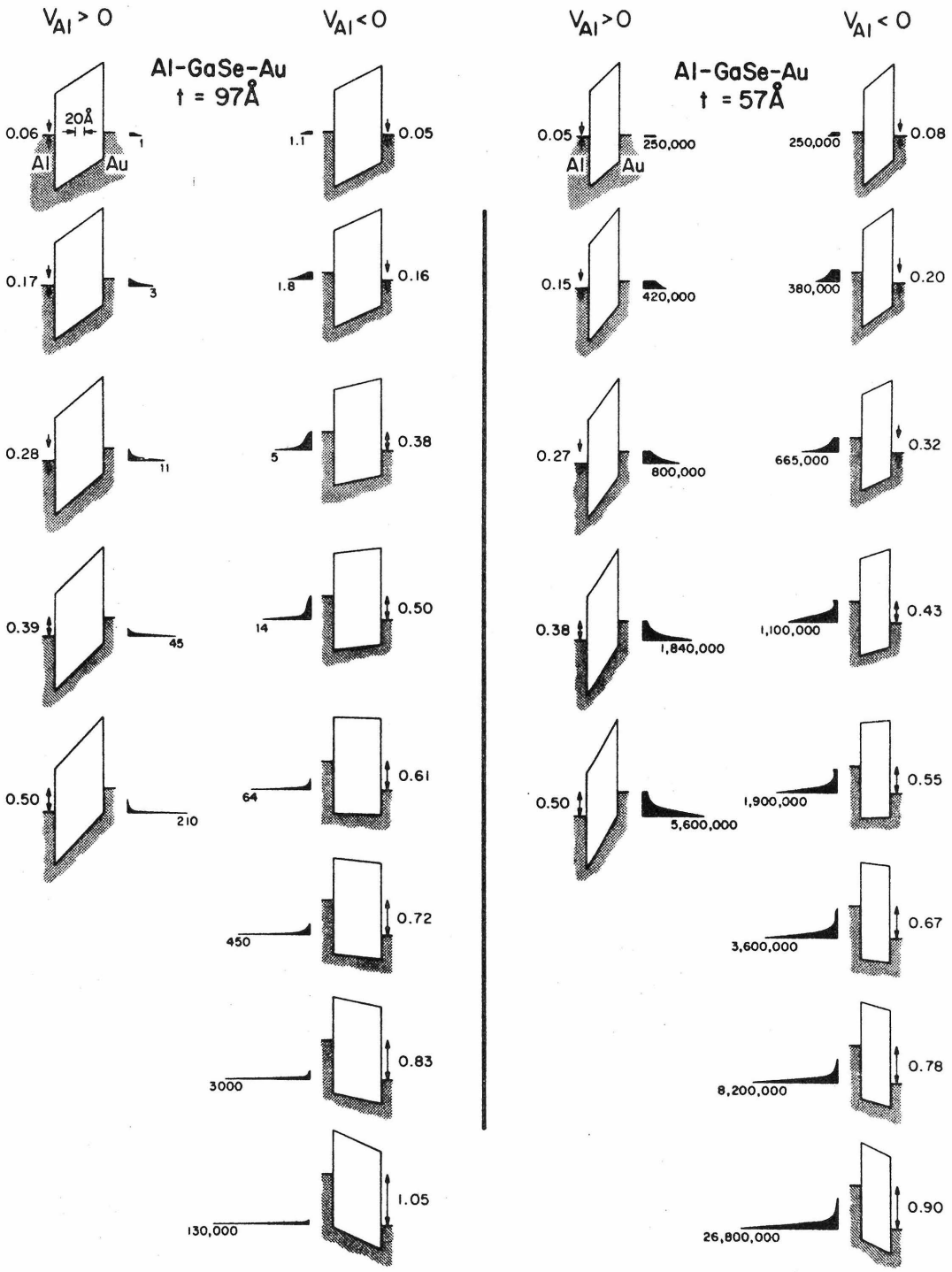
$V_{Al} > 0$
$V_{Al} < 0$
Al-GaSe-Au
t = 97Å
20Å
Al
Au
0.06
1
1.1
0.05
0.17
3
1.8
0.16
0.28
11
5
0.38
0.39
45
14
0.50
0.50
210
64
0.61
450
0.72
3000
0.83
130,000
1.05
$V_{Al} > 0$
$V_{Al} < 0$
Al-GaSe-Au
t = 57Å
0.05
250,000
250,000
0.08
0.15
420,000
380,000
0.20
0.27
800,000
665,000
0.32
0.38
1,840,000
1,100,000
0.43
0.50
5,600,000
1,900,000
0.55
3,600,000
0.67
8,200,000
0.78
26,800,000
0.90

Fig. II.8

Fig. II.8 Energy distributions of tunneling electrons and corresponding band diagrams for two Al-GaSe-Au structures. These distributions were calculated using the techniques of Section II and give insight into the origin of tunneling current. All distributions are plotted on linear scales so that a visual estimate of the width of the distribution is meaningful. The number beneath the peak of each distribution indicates the absolute magnitude of that peak relative to the peak of every other distribution in the figure.

For the 97 Å structure, the width of the distribution (shaded curve) diminishes rapidly with increasing applied bias. However, for the 57 Å structure rather broad tunneling distributions are noted at all bias values. This distinction occurs because the thicker the sample, the more strongly the current distribution is weighted toward low values of k. The lack of appreciable curvature in the $E(k)$ relation for $E > 0.6$ eV (see Fig. II.5) gives rise to unusually broad tunneling distributions near zero bias, even for relatively thick specimens of GaSe.

significant depends, in general, on the curvature of the E-k relation. For GaSe this curvature is rather small for large energy and, consequently, electron tunneling through mid gap can be a major contribution to the total current.

It is interesting to note that the technique of Stratton et al, which is based on a distribution of carriers sharply peaked about the Fermi level of the source electrode, would have been inadequate and inappropriate for the calculation of tunneling currents in GaSe. This conclusion could have been inferred from the lack of self-consistency which would have resulted had that approach been used,[33] but may be directly drawn from Fig. II.8. The numerical technique of Section II.2 includes all contributions to the total tunneling-current and hence is more general than the technique of Stratton[12] in the sense that no assumption need be made about the nature of the E-k curve.

II.5 CONCLUSIONS

We have studied current flow in metal-insulator-metal structures incorporating single crystal films of GaSe less than 100Å thick. The dominant mechanism of current flow in these structures is direct inter-electrode tunneling through a trapezoidal potential barrier. Identification of this mechanism is based on quantitative comparison between experimental data and theoretical predictions calculated from the known properties of bulk GaSe.

The E-k dispersion relation within the forbidden gap of GaSe was calculated from a small subset of the data obtained and is shown to be intrinsic to GaSe. Knowledge of this relation, the properties of the bulk insulator, and the geometry of a given structure are sufficient to quantitatively predict tunneling currents and their dependence on applied bias, insulator thickness, and metal-insulator barrier energy. We therefore conclude that a single one-electron model of tunneling is an appropriate and sufficiently accurate description of current flow in those physical situations where the criteria for its applicability are fulfilled. These criteria are straightforward and can be examined a priori if the structure under study is well-defined and the relevant electronic properties of its constituents known.

Tunneling measurements provide a direct technique for measuring the energy-momentum dispersion relation within the forbidden gap of an insulator. This relation represents fundamental information about a given solid which cannot be obtained by other methods.

II.R REFERENCES

1. A. Sommerfeld and H. Bethe, Handbuch der Physik von Gierger und (Julius Springer-Verlag, Berlin, 1933) Vol. 24/2, p. 450f.
2. C. B. Duke, Tunneling in Solids, (Academic Press, New York, 1969).
3. C. A. Mead, Some Properties of Exponentially Damped Wavefunctions, Tunneling Phenomena in Solids (Plenum Press, 1969) Chapt. 9.
4. R. M. Handy, Phys. Rev. 126, 1968 (1962).
5. J. C. Fisher and I. Grover, J. Appl. Phys. 32, 172 (1961).
6. G. T. Advani et al, Proc. IRE, 1530 (1962).
7. D. Meyerhoffer and S. A. Ochs, J. Appl. Phys. 34 2535 (1963).
8. R. Holm, J. Appl. Phys. 22, 569 (1951).
9. M. McColl and C. A. Mead, Trans. Met. Soc. of AIME 233, 502 (1965); see also: M. McColl, Ph.D. Thesis, Calif. Inst. of Tech. 1964 (Unpublished).
10. G. A. Lewicki and C. A. Mead, Phys. Rev. Lett. 16, 21 (1966).
11. G. W. Lewicki and C. A. Mead, J. Phys. Chem. Solids 29, 1255 (1968).
12. R. Stratton, G. Lewicki and C. A. Mead, J. Phys. Chem. Solids 27, 1599 (1966).
13. J. Bardeen, Phys. Rev. Letters 6, 57 (1961).
14. M. H. Cohen, L. M. Falicov and J. C. Phillips, Phys. Rev. Letters 8, 316 (1962).
15. E. Burstein and S. Lundqvist, ed. Tunneling Phenomena in Solids, (Plenum Press, 1969).

16. W. A. Harrison, Phys. Rev. 123, 85 (1961).

17. T. C. McGill, Ph.D. Thesis, Calif. Inst. of Tech. 1969; available from University Microfilms, Ann Arbor, Michigan.

18. V. Heine; Proc. Phys. Soc. 81, 300 (1963).

19. E. I. Blount Solid State Physics (Vol. 13 Academic Press, New York Appendix C.

20. Hence, the error caused by this assumption can be estimated only after an E-k curve is computed and the actual energy distribution of tunneling electrons is available.

21. The modifications to the barrier potential due to image force lowering could be incorporated into this equation without essentially modifying the results. Previous experience has shown that its effect is small when the low frequency dielectric constant is used. See: K. K. Thornber, T. C. McGill, C. A. Mead, J. Appl. Phys. 38, 2384 (1967).

22. ϕ_1 is taken to be less than ϕ_2.

23. H. A. Antosiewicz and W. C. Rheinboldt Survey of Numerical Analysis (McGraw-Hill Book Company, New York 1962, Chapt. 14, pp. 512-514).

24. Numerical techniques used in this calculation are more fully discussed in Ref. 17.

25. J. Franklin, J. Math. Analysis and Applications 30, (1970).

26. D. P. Foote and B. Kazan, Report #ASD-TDR-63-640, Electro-Optical Systems, Inc., Pasadena, Calif., August (1963).

27. P. Fielding, A. Fisher, and E. Mooser, J. Phys. Chem. Solids 8, 434 (1959); J. L. Brebner, J. Phys. Chem. Solids, 25 (1427) 1964; R. H. Bube and E. L. Lind, Phys. Rev. 115, 1159 (1959).

28. T. C. McGill, S. Kurtin and C. A. Mead, J. Appl. Phys.41,3831(1970).

29. If the optical value of the dielectric constant is used, the image force lowering is still less than 35 meV.

30. The assistance of M. Simpson in the fabrication of this viewer is gratefully acknowledged.

31. More rigorously the barrier shape may be any specific function of t/t_o, but physical arguments based on the inherent uniformity of single crystal films and the possible edge effects occuring at the metal-insulator interface collapse this class of functions into the trapezoidal case.

32. As a practical matter, a well prepared substrate may contain several small regions of five to fifteen structures each with nearly the same capacitance. Experience indicates that such a region contains at its center structures whose insulator thickness is uniform.

33. This sort of inconsistency was noticed by Lewicki (G. W. Lewicki, Ph.D. Thesis, Calif. Inst. of Tech. 1966; available from University Microfilms, Ann Arbor, Michigan) in his study of Au-AlN-Al structures and attributed to wide tunneling distributions. The techniques discussed herein have been applied to Lewicki's data with notable success (see Ref. 17).